

**A time-varying parameter estimation approach using split-sample  
calibration based on dynamic programming**

**Xiaojing Zhang<sup>a,b</sup>, Pan Liu<sup>a,b\*</sup>**

<sup>a</sup>State Key Laboratory of Water Resources and Hydropower Engineering Science, Wuhan University,  
Wuhan 430072, China

<sup>b</sup>Hubei Provincial Key Lab of Water System Science for Sponge City Construction, Wuhan  
University

\*Corresponding author. Email: liupan@whu.edu.cn;

Tel: +86-27-68775788; Fax: +86-27-68773568

1 **Abstract:** Although the parameters of hydrological models are usually regarded as  
2 constant, temporal variations can occur in a changing environment. Thus, effectively  
3 estimating time-varying parameters becomes a significant challenge. Two methods,  
4 including split-sample calibration (SSC) and Data assimilation, have been used to  
5 estimate time-varying parameters. However, SSC is unable to consider the parameter  
6 temporal continuity, while Data assimilation assumes parameters vary at every time-  
7 step. This study proposed a new method that combines (1) the basic concept of split-  
8 sample calibration (SSC), whereby parameters are assumed to be stable for one sub-  
9 period, and (2) the parameter continuity assumption, i.e., the differences between  
10 parameters in consecutive time steps are small. Dynamic programming is then used to  
11 determine the optimal parameter trajectory by considering two objective functions:  
12 maximization of simulation accuracy and maximization of parameter continuity. The  
13 efficiency of the proposed method is evaluated by two synthetic experiments, one with  
14 a simple two-parameter monthly model and the second using a more complex 15-  
15 parameter daily model. The results show that the proposed method is superior to SSC  
16 alone, and outperforms the ensemble Kalman filter if the proper sub-period length is  
17 used. An application to the Wuding River basin indicates that the soil water capacity  
18 parameter varies before and after 1972, which can be interpreted according to land use  
19 and land cover changes. A further application to the Xun River basin shows that  
20 parameters are generally stationary on an annual scale, but exhibit significant changes  
21 over seasonal scales. These results demonstrate that the proposed method is an effective  
22 tool for identifying time-varying parameters in a changing environment.

23 **Keywords:** hydrological model; time-varying parameter; calibration; dynamic  
24 programming

## 25 **1. Introduction**

26        Conceptual models describe the physical processes that occur in the real world by  
27 means of certain assumptions and empirically determined functions (Toth and Brath,  
28 2007). In spite of their simplicity, conceptual models are effective in providing reliable  
29 runoff predictions for widespread applications (Quoc Quan et al., 2018; Refsgaard and  
30 Knudsen, 1996), such as real-time flood forecasting, climate change impact  
31 assessments (Deng et al., 2019; Stephens et al., 2019), and water resources management.  
32 Conceptual hydrological models typically have several inputs, a moderate number of  
33 parameters, state variables, and outputs. Among these, the parameters play an important  
34 role in accurate simulation and should be related to the catchment properties. However,  
35 parameter values often cannot be obtained by field measurements (Merz et al., 2011).  
36 An alternative approach is to calibrate parameters based on historical data.

37        Parameters are usually regarded as constants in time scale, because of the general  
38 idea that catchment conditions are temporally stable. Constant parameters become  
39 inaccurate in differential split-sample test (DSST) conditions (Klemes, 1986). For  
40 example, parameters calibrated based on data from a wet (or dry) period may fail to  
41 simulate runoff in a dry (or wet) period for the same catchment. Broderick et al. (2016)  
42 used DSST to assess the transferability of six conceptual models under contrasting  
43 climate conditions. They found that performance declines most when models are  
44 calibrated during wet periods but validated in dry ones. Fowler et al. (2016) pointed out  
45 that the parameter set obtained by mathematical optimization based on wet periods may  
46 not be robust when applied in dry periods. Additionally, the catchment properties can

47 change over time, such as in the case of afforestation and deforestation (Guzha et al.,  
48 2018; Siriwardena et al., 2006). These changes need to be taken into account through  
49 model parameters (Bronstert, 2004; Hundecha and Bardossy, 2004). Hence, temporal  
50 variations in parameters should reflect the changing environment.

51 One challenge here is the methodology used to identify time-varying parameters.  
52 In the literature, three approaches have been discussed. The first is split-sample  
53 calibration (SSC), whereby available data are split into a moderate number of sub-  
54 periods and the parameters are calibrated individually for each period (Thirel et al.,  
55 2015). The second method is data assimilation (Deng et al., 2016; Pathiraja et al., 2018).  
56 This method assimilates observational data to enable errors, states, and parameters to  
57 be updated (Li et al., 2013), making it possible to identify time-varying parameters. The  
58 third approach is to construct a functional form or empirical equation according to the  
59 correlation between parameters and some climatic variates such as precipitation and  
60 potential evapotranspiration (Deng et al., 2019; Jeremiah et al., 2013; Westra et al.,  
61 2014). Note that this study focuses on methods to identify time-varying parameters  
62 rather than modelling them; hence, only comparisons between SSC and data  
63 assimilation are discussed.

64 SSC is the most commonly used method (Coron et al., 2012; Fowler et al., 2018;  
65 Paik et al., 2005; Xie et al., 2018). Merz et al. (2011) investigated the time stability of  
66 parameters by estimating six parameter sets based on six consecutive five-year periods.  
67 Lan et al. (2018) clustered calibration data into 24 sub-annual periods to detect the  
68 seasonal hydrological dynamic behavior. Despite broad application, it remains



69 debatable whether a particular mathematical optimum gives the parameter value during  
70 one period. Many equivalent optima can exist simultaneously for one dataset when  
71 calibrating the model against observations (Poulin et al., 2011). Several studies  
72 addressed this question by adding more constraints to the objective function over the  
73 respective period. For example, Gharari et al. (2013) emphasized consistent  
74 performance in different climatic conditions, while Xie et al. (2018) modified SSC by  
75 selecting parameters with good simulation ability for both the current sub-period and  
76 the whole period. Some conceptual hydrological parameters reflect the catchment  
77 characteristics. While climate change and human activities exert influence on these  
78 catchment characteristics, they can hardly change dramatically in a very quick time,  
79 such as the soil water storage capacity. Hence, parameter continuity, defined as  
80 differences between the parameters in consecutive time steps to be small, is required  
81 for hydrological modeling. However, few reports have considered the continuity of  
82 parameters in the SSC method.

83 ~~Continuity requires differences between the parameters in consecutive time steps~~  
84 ~~to be small. Some conceptual hydrological parameters reflect the catchment~~  
85 ~~characteristics. While climate change and human activities exert influence on these~~  
86 ~~catchment characteristics, they can hardly change dramatically in a very quick time,~~  
87 ~~such as the soil water storage capacity.~~ This assumption of parameter continuity is the  
88 basic idea behind data assimilation methods. For example, the a priori parameters in  
89 ensemble Kalman filter (EnKF) methods are commonly derived from updated values  
90 from the previous time step (Moradkhani et al., 2005; Xiong et al., 2019). From this, a

设置了格式: 字体: 非加粗, 字体颜色: 自动设置

91 trade-off between simulation accuracy and parameter continuity is established, and  
92 parameters that enable greater continuity are more likely to be selected. Deng et al.  
93 (2016) validated the ability of the EnKF to identify changes in two-parameter monthly  
94 water balance (TMWB) model parameters. Pathiraja et al. (2016) proposed two-  
95 parameter evolution models for improving conventional dual EnKF, and obtained  
96 superior results for diagnosing the non-stationarity in a system. EnKF and its variants  
97 are relatively advanced approaches for identifying time-varying parameters (Lu et al.,  
98 2013). However, for a hydrological model, the states may change over every time step,  
99 whereas the parameters may not, in particular for hourly time scales. This can be offset  
100 by SSC, which assumes that the parameters remain stable for a pre-determined period  
101 (such as decades, years, or months). Compared to EnKF, the simplicity of SSC is  
102 another advantage, as it has a less complex mechanism and reduced redundancy (Chen  
103 and Zhang, 2006).

104 The aim of this study is to present a new method for time-varying parameter  
105 estimation by combining the strengths of the basic concept of SSC and the continuity  
106 assumption of data assimilation, which is a useful tool for diagnosing the non-  
107 stationarity caused by a changing environment. Compared with data assimilation, the  
108 proposed split-sample calibration based on dynamic programming (SSC-DP) avoids  
109 overly frequent changes of parameters, such as hourly or daily variations. Compared  
110 with SSC, the distinctive element is that SSC-DP considers the parameters to be related  
111 over adjacent sub-periods, and selects parameter sets with good performance for each  
112 period and small differences between adjacent time steps. In this study, three aspects of

113 the proposed method are evaluated: (1) The performance of SSC-DP is compared with  
114 that of existing methods in terms of the estimation of time-varying parameters; (2) The  
115 applicability of SSC-DP to more complex hydrological models with a considerable  
116 number of parameters; (3) The ability of SSC-DP to provide additional insights on  
117 parameter variations and their correlations with the properties of real catchments. To  
118 investigate the above issues, the proposed method is compared with SSC and EnKF in  
119 two synthetic experiments (one with a two-parameter monthly model, the other with a  
120 15-parameter daily model). SSC-DP is also applied to two real catchments for  
121 parameter estimation under different environmental conditions.

122 The remainder of this paper is organized as follows. Section 2 describes the  
123 proposed method, reference methods, and performance evaluation indices. Section 3  
124 describes two synthetic experiments and two real catchment case studies for  
125 comparison among different time-varying parameter estimation methods. Sections 4  
126 and 5 present the results and discussion, respectively, before the conclusions to this  
127 study are drawn in Sect. 6.

## 128 **2. Methodology**

129 In this section, a SSC-DP method is proposed to identify the time-varying  
130 parameters of hydrological models. The two hydrological models considered in this  
131 study are the TMWB and Xinanjiang models. Their concepts and differences are  
132 presented in Sect. 2.1. A sensitivity analysis is employed to focus efforts on parameters  
133 important to calibration and avoid prohibitive computational cost, as outlined in Sect.  
134 2.2. Three time-varying parameter estimation methods (SSC, SSC-DP, and data

135 assimilation) are presented in Sect. 2.3. The SSC and data assimilation are provided for  
136 comparisons with the SSC-DP. Finally, to evaluate the performance of the time-varying  
137 parameter estimation methods, six evaluation criteria are selected and formulated in  
138 Sect. 2.4. The flowchart of the methodologies is shown in Fig. 1.

## 139 **2.1 Hydrological models**

### 140 **2.1.1 Two-parameter monthly water balance model**

141 The TMWB model developed by Xiong and Guo (1999) is efficient for monthly  
142 runoff simulations and forecasts (Dai et al., 2018; Guo et al., 2002; Kim et al., 2016;  
143 Yang et al., 2017). The model requires monthly precipitation and potential  
144 evapotranspiration as inputs. Its simplicity and efficiency of performance mean that  
145 TMWB can easily be used to investigate the impacts of climate change (Deng et al.,  
146 2016; Luo et al., 2019). Its outputs include monthly streamflow, actual  
147 evapotranspiration, and soil moisture content index. The model has only two  
148 parameters (Table 1),  $C$  and  $SC$ . The parameter  $C$  takes account of the effect of the  
149 change of time scale when simulating actual evapotranspiration. The parameter  $SC$   
150 represents the field capacity (mm).

### 151 **2.1.2 Xinanjiang model**

152 The Xinanjiang model (Zhao, 1992) is widely used in China (Li and Zhang, 2017;  
153 Si et al., 2015; Yin et al., 2018). It takes precipitation and pan-evaporation data as inputs  
154 and estimates the actual evapotranspiration, soil moisture storage, surface runoff,  
155 interflow, and groundwater runoff from the watershed. The simulated streamflow is

156 calculated by summing the routing results of the surface, interflow, and groundwater  
 157 runoff (Sun et al., 2018). In this study, the surface runoff is routed by the instantaneous  
 158 unit hydrograph (Lin et al., 2014), while the interflow and groundwater runoff are  
 159 routed by the linear reservoir method (Jayawardena and Zhou, 2000). A schematic  
 160 overview of the model is presented in Fig. 2. The meaning, range and units of all the  
 161 parameters in the Xinanjiang model are listed in Table 2.

162 There are two important differences between the TMWB and Xinanjiang models:  
 163 (1) the TMWB model has two parameters, while the Xinanjiang model has fifteen  
 164 parameters; (2) TMWB is a monthly rainfall-runoff model, whereas the Xinanjiang  
 165 model can run on hourly or daily step sizes.

## 166 2.2 Parameter sensitivity analysis method

167 Sensitivity analysis is used to identify which parameters significantly affect the  
 168 performance of the Xinanjiang model and reduce the number of parameters to be  
 169 calibrated. Numerous sensitivity analysis methods are available, such as the Morris  
 170 method (Morris, 1991) and Sobol analysis (Sobol, 1993). The Morris method provides  
 171 similar results to Sobol analysis with a reduced computational burden (Rebolho et al.,  
 172 2018; Teweldebrhan et al., 2018; Yang et al., 2018).

173 The Morris method assumes that if parameters change by the same relative amount,  
 174 the parameter that causes the larger elementary effect is the more sensitive (King and  
 175 Perera, 2013). The elementary effect is calculated as follows:

$$176 \quad EE_p(\theta_1, \theta_2, \dots, \theta_{Np}, \Delta) = \frac{y(\theta_1, \theta_2, \dots, \theta_{p-1}, \theta_p + \Delta, \theta_{p+1}, \dots, \theta_{Np}) - y(\theta_1, \theta_2, \dots, \theta_{Np})}{\Delta} \quad (1)$$

177 where  $\theta_p$  represents the  $p$ -th parameter;  $\Delta$  is the relative amount;  $Np$  is the total  
178 number of parameters, and  $y$  is the model output based on a particular parameter set.

179 Each parameter is changed in turn and every parameter set produces an elementary  
180 effect. The parameter sensitivity is evaluated using the mean value  $\mu$  of the  
181 elementary effects. If a parameter has a higher value of  $\mu$ , it is more sensitive. In fact,  
182 interactions between parameters should be taken into account (Jie et al., 2018). Hence,  
183 the standard deviation  $\sigma$  can be calculated. A higher value of  $\sigma$  indicates a stronger  
184 nonlinear correlation between parameters (Pappenberger et al., 2008).

## 185 **2.3 Time-varying parameter estimation method**

### 186 **2.3.1 Split-sample calibration**

187 SSC provides a simple way of diagnosing parameter non-stationarity under a  
188 changing environment (Merz et al., 2011). As illustrated in Fig. 3(a), the method usually  
189 has two steps (Hughes, 2015; Kim et al., 2015): (1) Available data are divided into  
190 several consecutive periods, which can be arbitrarily chosen as hours, days, months,  
191 seasons, or years; (2) Parameters are calibrated separately for the respective period.  
192 This procedure gives better simulation performance than using constant parameters, but  
193 leads to the estimated parameters fluctuating strongly over adjacent sub-periods,  
194 producing false temporal variants.

### 195 **2.3.2 Split-sample calibration based on dynamic programming**

196 To overcome this problem, the SSC-DP method identifies time-varying parameters  
197 with consideration of temporal continuity. SSC-DP has five steps (Fig. 3(b)):

198 (1) Split-sample periods. This process is the same as the first step of the SSC.

199 (2) Generate an ensemble of near-optimal parameters. Multiple parameter sets  
 200 having objective values close to the optimum for each sub-period are obtained using  
 201 Markov chain Monte Carlo (MCMC) sampling.~~Feasible parameter space generation. An~~  
 202 ~~ensemble of nearly optimal parameter sets for each sub-period is obtained using~~  
 203 ~~Markov chain Monte Carlo (MCMC) sampling~~ (Chib and Greenberg, 1995). The  
 204 likelihood measure of the  $i$ -th sub-period links the parameter to observations using the  
 205 Nash–Sutcliffe efficiency (NSE) (Nash and Sutcliffe, 1970) as follows:

$$206 \quad L_i(\theta) = 1 - \frac{\sum_{t=(i-1)l+1}^{i \cdot l} (Q_t - \hat{Q}_t)^2}{\sum_{t=(i-1)l+1}^{i \cdot l} (Q_t - \bar{Q}_i)^2} \quad (2)$$

207 where  $Q_t$  and  $\hat{Q}_t$  are the observed and simulated runoff at time step  $t$ , respectively,  
 208 and  $l$  is the length of the sub-period.

209 (3) Optimize by using Dynamic programming. The goal is to find parameters that  
 210 provide both accurate streamflow simulations and continuity.~~Dynamic programming~~  
 211 ~~optimization. The goal is to find parameters that provide both good model performance~~  
 212 ~~and continuity.~~ The continuity condition aims to minimize the difference between the  
 213 estimated parameters for sub-periods  $i$  and  $i+1$ . For  $N$  sub-periods, the objective  
 214 function can be expressed as follows:

$$215 \quad \text{Max } F = \sum_{i=1}^N [(NSE_i + NSE_{ln,i} + NSE_{abs,i}) - \alpha \times \sum_{p=1}^{N_p} \frac{|\theta_{i+1,p} - \theta_{i,p}|}{\theta_{max,p} - \theta_{min,p}}] \quad (3)$$

$$216 \quad NSE_{ln,i} = 1 - \frac{\sum_{t=(i-1)l+1}^{i \cdot l} (\ln(Q_t) - \ln(\hat{Q}_t))^2}{\sum_{t=(i-1)l+1}^{i \cdot l} (\ln(Q_t) - \ln(\bar{Q}_i))^2} \quad (4)$$

217

$$NSE_{abs,i} = 1 - \frac{\sum_{t=(i-1) \times l+1}^{i \times l} |Q_t - \widehat{Q}_t|}{\sum_{t=(i-1) \times l+1}^{i \times l} |Q_t - \overline{Q}_t|} \quad (5)$$

218 where  $\theta_{i,p}$  is the  $p$ -th estimated parameter over the  $i$ -th sub-period;  $\theta_{max,p}$  and  
 219  $\theta_{min,p}$  are its maximum and minimum values, respectively;  $N_p$  is the number of the  
 220 parameters; and  $\alpha$  is the weight, reflecting parameter continuity. The weights of  
 221  $NSE_i$ ,  $NSE_{ln,i}$ , and  $NSE_{abs,i}$  are set to 1 following the work of Merz et al. (2011), who  
 222 used equal weights for the NSE and its variants.

223 As the decision-making process during the current sub-period is related to that of  
 224 the previous sub-period, the parameter estimation over  $N$  periods becomes a multi-stage  
 225 optimization problem. To solve this, a dynamic programming technique (Bellman, 1957)  
 226 is employed to decompose the optimization into a number of single-stage problems and  
 227 determine the optimal trajectory of the time-varying parameters. Dynamic  
 228 programming is a useful method for handling sequential operation decisions. It allows  
 229 the problem to be solved using a backward recursive procedure, whereby the decision-  
 230 making for each sub-period maximizes the sum of current and future benefits (Li et al.,  
 231 2018; Ming et al., 2017). In this study, the objective function is formulated as the  
 232 following recursive equation:

$$\begin{cases} F_i^* = \max\{f_i[\vartheta_{i,1}, \vartheta_{i,2}, \vartheta_{i,3}, \dots, \vartheta_{i,p}] + F_{i+1}^*\} \\ F_N^* = 0 \end{cases} \quad (6)$$

234 where  $F_i^*$  is the evaluation index using the optimal time-varying parameters from the  
 235  $N$ -th to the  $i$ -th sub-periods, and Eq. (6) calculates the objective function from the  $N$ -th  
 236 sub-period to the first sub-period.



237 (4) Update initial states. The initial states, such as that of the soil water content,  
238 are important in model simulation and calibration. As the final states for sub-period  $i$   
239 are not used as the initial states for sub-period  $i+1$  during steps (1)–(3), the time-varying  
240 parameter set obtained from step (3) is applied to the hydrological model to update the  
241 initial states of each sub-period for the next iteration.

242 (5) Steps (1)–(4) are repeated until the initial states of each sub-period are  
243 generally stable.

### 244 **2.3.3 Data assimilation**

245 Another approach for diagnosing variations in parameters is data assimilation,  
246 using methods such as the EnKF and ensemble Kalman smoother (EnKS). These are  
247 used here as reference methods. The EnKF has been widely applied to conceptual  
248 models, including TMWB (Deng et al., 2016). Li et al. (2013) noted that the EnKF  
249 struggles to handle the time-lag in routing processes. However, the routing component  
250 is vital to the Xinanjiang model. EnKS can efficiently determine the states of the  
251 Xinanjiang model (Meng et al., 2017), but the estimation of routing parameters deserves  
252 discussion. Most previous studies have used a fixed distribution of the routing  
253 hydrograph in data assimilation (Lu et al., 2013), i.e., the parameters are constant for  
254 routing processes. With respect to these issues, a modified EnKF (named SSC-EnKF)  
255 is established as a third data assimilation reference method in the synthetic experiment  
256 with the Xinanjiang model (described in Sect. 3.1).

257 The EnKF includes two main steps: model prediction and assimilation. The state  
258 vector is augmented with parameter variables so that time-varying parameters can be

259 estimated simultaneously with model states. For model prediction, the augmented  
 260 vector is derived by adding noise on that from the previous time step through the  
 261 following equation:

$$262 \quad \begin{pmatrix} \mathcal{G}_{t+1}^{k-} \\ \mathcal{X}_{t+1}^{k-} \end{pmatrix} = \begin{pmatrix} \mathcal{G}_t^{k+} \\ f(\mathcal{X}_t^{k+}, \theta_{t+1}^{k-}, \mathbf{u}_{t+1}) \end{pmatrix} + \begin{pmatrix} \delta_t^k \\ \varepsilon_t^k \end{pmatrix}, \quad \delta_t^k \sim N(0, R_t), \varepsilon_t^k \sim N(0, G_t) \quad (7)$$

263 where  $\mathcal{g}_t$  is the parameter vector at time step  $t$ , represented as  $(\theta_{t,1}, \theta_{t,2}, \dots, \theta_{t,N_p})$ ;  $x_t$   
 264 is the state vector;  $\mathcal{G}_{t+1}^{k-}$  and  $\mathcal{X}_{t+1}^{k-}$  are the  $k$ -th ensemble member forecasts at time step  
 265  $t+1$ ;  $\mathcal{G}_t^{k+}$  and  $\mathcal{X}_t^{k+}$  are the updated values of the  $k$ -th ensemble member forecasts at time  
 266 step  $t$ ;  $u_{t+1}$  denotes the forcing data (e.g., precipitation) at time step  $t+1$ ;  $\delta_t^k$  and  $\varepsilon_t^k$   
 267 are the white noise for the  $k$ -th ensemble member, which follow a Gaussian distribution  
 268 with zero mean and specified covariance of  $R_t$  and  $G_t$ , respectively.

269 In the assimilation process, the augmented vector is updated using the following  
 270 equations if suitable observations are available:

$$271 \quad \begin{pmatrix} \mathcal{X}_{t+1}^{k+} \\ \mathcal{G}_{t+1}^{k+} \end{pmatrix} = \begin{pmatrix} \mathcal{X}_{t+1}^{k-} \\ \mathcal{G}_{t+1}^{k-} \end{pmatrix} + \begin{pmatrix} K_{t+1}^x [y_{t+1}^k - \hat{y}_{t+1}^k] \\ K_{t+1}^g [y_{t+1}^k - \hat{y}_{t+1}^k] \end{pmatrix} \quad (8)$$

$$272 \quad y_{t+1}^k = y_{t+1} + \xi_{t+1}^k, \quad \xi_{t+1}^k \sim N(0, W_t), \quad (9)$$

$$273 \quad \hat{y}_{t+1}^k = h(\mathcal{X}_{t+1}^{k-}, \mathcal{G}_{t+1}^{k-}) \quad (10)$$

274 where  $y_{t+1}$  is the observation vector at time  $t+1$ ;  $y_{t+1}^k$  is the  $k$ -th observation  
 275 ensemble member at time step  $t+1$ ;  $\hat{y}_{t+1}$  is the simulation vector at time  $t+1$ ;  $h$  is the  
 276 observational operator that converts the model states to observations;  $\xi_{t+1}^k$  is the  
 277 measurement error, which follows a Gaussian distribution with a covariance of  $W_t$ ; and  
 278  $K_{t+1}^k$  is the Kalman gain matrix (for details, see (Feng et al., 2017)).

279 The EnKS is based on the EnKF. Whereas the EnKF updates the model states and

280 parameters at the current time step, the EnKS takes account of those values over the  
 281 past time steps. The main steps of the EnKS are identical to those of the EnKF, but the  
 282 equation of the assimilation process is formulated as follows:

$$283 \begin{pmatrix} x_{t+1 \rightarrow t-n+2}^{k+} \\ \mathcal{G}_{t+1 \rightarrow t-n+2}^{k+} \end{pmatrix} = \begin{pmatrix} x_{t+1 \rightarrow t-n+2}^{k-} \\ \mathcal{G}_{t+1 \rightarrow t-n+2}^{k-} \end{pmatrix} + \begin{pmatrix} K_{t+1}^{x*} [y_{t+1}^k - \hat{y}_{t+1}^k] \\ K_{t+1}^{g*} [y_{t+1}^k - \hat{y}_{t+1}^k] \end{pmatrix} \quad (11)$$

$$284 \hat{y}_{t+1}^k = h(x_{t+1 \rightarrow t-n+2}^{k-}, \mathcal{G}_{t+1 \rightarrow t-n+2}^{k-}) \quad (12)$$

285 where  $K_{t+1}^{x*}$  is the Kalman gain matrix of EnKS. The fixed time window  $n$  of EnKS  
 286 is pre-determined based on the response function or unit hydrograph. Meng et al.  
 287 (2017) suggested that the time window should be set as half of the recession time of  
 288 a flood.

289 A third data assimilation approach is constructed based on the SSC. Instead of  
 290 assimilating one observed variable, it assimilates the observed variables during a given  
 291 period in one assimilation process. Assuming that the parameters are constant in the  
 292 given period, the equation of the assimilation process for the  $i$ -th sub-period is  
 293 expressed as follows:

$$294 \begin{pmatrix} x_{i+1}^{k+} \\ \mathcal{G}_{i+1}^{k+} \end{pmatrix} = \begin{pmatrix} x_{i+1}^{k-} \\ \mathcal{G}_{i+1}^{k-} \end{pmatrix} + \begin{pmatrix} K_{i+1}^{x*} [y_{i \times l+1 \rightarrow (i+1) \times l}^k - \hat{y}_{i \times l+1 \rightarrow (i+1) \times l}^k] \\ K_{i+1}^{g*} [y_{i \times l+1 \rightarrow (i+1) \times l}^k - \hat{y}_{i \times l+1 \rightarrow (i+1) \times l}^k] \end{pmatrix} \quad (13)$$

$$295 \hat{y}_{i \times l+1 \rightarrow (i+1) \times l}^k = h(x_{i+1}^{k-}, \mathcal{G}_{i+1}^{k-}) \quad (14)$$

296 where  $\mathcal{g}_i$  is the parameter vector for sub-period  $i$ , represented as  $(\theta_{i,1}, \theta_{i,2}, \dots, \theta_{i,Np})$ ;  
 297  $x_i$  is the initial state vector for sub-period  $i$ ; and  $l$  is the length of the sub-period.

298 This approach addresses the routing-lag issue by allowing parameters of the  
 299 routing processes, such as the instantaneous unit hydrograph, to remain constant for  
 300 each sub-period and to be time-varying over the whole period.

301 **2.4 Model evaluation criteria**

302 The streamflow simulations given by the proposed method are verified using the  
303 NSE, relative error (RE) and NSE on logarithm of streamflow (NSE<sub>ln</sub>) (Hock, 1999).  
304 RE evaluates the error of the total volume of streamflow, while NSE and NSE<sub>ln</sub>  
305 evaluate the agreement between the hydrograph of observations and simulations. NSE  
306 is more sensitive to high flows, but NSE<sub>ln</sub> focuses more on low flows. Higher values  
307 of NSE, NSE<sub>ln</sub> and lower absolute values of RE indicate better streamflow simulations.  
308 The NSE, RE and NSE<sub>ln</sub> are expressed as followed:

309 
$$NSE = 1 - \frac{\sum_{t=1}^m (Q_t - \hat{Q}_t)^2}{\sum_{t=1}^m (Q_t - \bar{Q})^2} \quad (15)$$

310 
$$RE = \frac{\sum_{t=1}^m (Q_t - \hat{Q}_t)}{\sum_{t=1}^m Q_t} \quad (16)$$

311 
$$NSE_{ln} = 1 - \frac{\sum_{t=1}^m (\ln(Q_t) - \ln(\hat{Q}_t))^2}{\sum_{t=1}^m (\ln(Q_t) - \ln(\bar{Q}))^2}$$

312 The estimated parameters are evaluated by the RMSE (Alvisi et al., 2006), MARE  
313 (Khalil et al., 2001) and R<sup>2</sup> (Kim et al., 2007) in the synthetic experiments (see details  
314 in section 3.1). RMSE is more sensitive to high values than MARE, while R<sup>2</sup> is based  
315 on the linear assumption. RMSE and MARE quantify the accuracy of the estimated  
316 parameters, but RMSE is more sensitive to high values than MARE. R<sup>2</sup> records the  
317 overall agreement between the true and estimated parameters (Dawson et al., 2007).

设置了格式: 上标

318 Smaller values of RMSE, MARE and higher values of  $R^2$  indicate stronger parameter  
 319 identification ability. For the  $p$ -th parameter, the formulations are as follows:

$$320 \quad RMSE_p = \sqrt{\frac{1}{m} \sum_{t=1}^m (\theta_{t,p} - \hat{\theta}_{t,p})^2} \quad (18)$$

$$321 \quad MARE_p = \frac{1}{m} \sum_{t=1}^m \frac{|\theta_{t,p} - \hat{\theta}_{t,p}|}{\theta_{t,p}} \quad (19)$$

$$322 \quad R^2_p = \frac{\sum_{t=1}^m (\hat{\theta}_{t,p} - \bar{\theta}_p)(\theta_{t,p} - \bar{\theta}_p)}{\sqrt{\sum_{t=1}^m (\hat{\theta}_{t,p} - \bar{\theta}_p)^2 (\theta_{t,p} - \bar{\theta}_p)^2}} \quad (20)$$

323 where  $\theta_t$  and  $\hat{\theta}_t$  are the true parameter and its estimated value at the  $t$ -th time step,  
 324 respectively;  $\bar{\theta}_p$  and  $\bar{\hat{\theta}}_p$  are the mean value of the true parameters and its estimated  
 325 values, respectively; and  $m$  is the length of the data during the whole period.

326

### 327 3. Synthetic experiment and real catchment case study

328 Two synthetic experiments and two real catchment case studies were designed to  
 329 assess the performance of SSC-DP. The experiments are described in Table 3.

#### 330 3.1 Synthetic experiments

331 The two synthetic experiments examine the ability of SSC-DP to identify the time-  
 332 varying parameters of the TMWB and Xinanjiang hydrological models. The merit of  
 333 synthetic experiments is that the parameters can be synthetically generated to be either  
 334 constant or time-varying. Hence, it is convenient to compare the estimated values with  
 335 the pre-determined parameters to evaluate different parameter estimation methods.

336 Note that synthetic experiments have been successfully used in several time-varying  
337 parameter identification studies (Deng et al., 2016; Pathiraja et al., 2016; Xiong et al.,  
338 2019).

### 339 **3.1.1 Synthetic experiment with the TMWB model**

340 Synthetic data of monthly precipitation and potential evapotranspiration were  
341 collected from the 03451500 catchment of the Model Parameter Estimation Experiment  
342 (MOPEX) (Duan et al., 2006). The data cover 252 months. Runoff was derived by the  
343 TMWB model using synthetic precipitation, potential evapotranspiration, and the pre-  
344 determined parameters. Gaussian noise was added to the simulated runoff to represent  
345 uncertainties. The mean of the noise was set to zero, and the standard deviation was  
346 assumed to be 3 % of the magnitude of the values (Deng et al., 2016).

347 Eight scenarios with different pre-determined parameters were investigated (Table  
348 4). The first scenario considered constant parameters. Scenarios 2 and 3 considered  
349 month-by-month variations in TMWB model parameters, i.e., the parameters remain  
350 constant during each month, but change from month to month. Scenarios 4 and 5  
351 considered parameters that change every six months. Scenarios 6–8 considered year-  
352 by-year variations. The changes in both  $C$  and  $SC$  were considered to be linear in  
353 scenarios 2, 4, and 6 (Trend) and sinusoidal in scenarios 3, 5 and 7 (periodicity),  
354 reflecting the impacts of climate change and human activities (Pathiraja et al., 2016).  
355 Scenario 8 considered a periodic variation with an increasing trend for parameter  $C$  and  
356 only the linear variation in  $SC$ .

### 357 3.1.2 Synthetic experiment with the Xinanjiang model

358 Hourly precipitation and pan evaporation data were collected from the Baiyunshan  
359 Reservoir basin in China. The data cover a period of 18000 h. The Xinanjiang model  
360 has 15 parameters, which can lead to a significant computational burden. To reduce the  
361 total number of model runs, only the sensitive parameters were considered to be free.  
362 The Morris method was used to detect the free parameters (Fig. 4), with the results  
363 showing that *KE*, *CI*, *CG*, *KI*, *KG*, and *NK* are sensitive parameters. Thus, the other  
364 parameters were held constant for the whole period.

365 Similar to the experiment with the TMWB model, the synthetic runoff was derived  
366 from the Xinanjiang model with added Gaussian noise. The mean of the noise was set  
367 to zero, and the standard deviation was assumed to be 5 % of the magnitude of the  
368 values. As presented in Table 5, all 15 parameters were set to be constant in the first  
369 scenario. The pre-determined sensitive parameters were considered to vary with a  
370 certain trend and periodicity in scenarios 2 and 3, respectively. Scenario 4 considered a  
371 combined variation of trend and periodicity for the parameter *KE*, with the other free  
372 parameters set to vary linearly. The parameter variations in scenarios 2–4 were assumed  
373 to occur once a month.

### 374 3.2 Study area: Wuding River basin

375 The Wuding River basin (Fig. 5(a)) examined in the first case study is a large sub-  
376 basin of the Yellow River basin located on the Loess Plateau (Xu, 2011). The Wuding  
377 River has a drainage area of 30261 km<sup>2</sup> and a total length of 491 km. The average slope

378 is 0.2 %, and the elevation varies from 600–1800 m above sea level. The area is a semi-  
379 arid region with mean annual precipitation of ~401 mm. The annual potential  
380 evapotranspiration is 1077 mm, and the mean annual runoff is 39 mm. The data for this  
381 basin were collected over the period 1958–2000. The daily precipitation was obtained  
382 from Thiessen polygons using records from 122 rain gauges. Based on meteorological  
383 data from the China Meteorological Data Sharing Service System (<http://data.cma.cn>),  
384 areal pan evaporation data were obtained. As illustrated in Fig. 5(a), the station furthest  
385 downstream, Baijiachuan, drains an area of 29,662 km<sup>2</sup> (98 % of the total basin) and  
386 records the daily runoff data. The data of the daily precipitation and streamflow in the  
387 Wuding River basin were obtained from the local Hydrology and Water Resources  
388 Bureau of China, the quality of which has been checked by the official authorities, and  
389 there are no gaps among these data for all the hydrological stations. It can be seen from  
390 Fig. 5(c) that the annual streamflow in the Wudinghe River basin has a distinct  
391 decreasing trend, while seasonal variations are not significant, but the annual  
392 precipitation and pan evaporation generally have no trend, suggesting the impacts of  
393 human activities on rainfall-runoff relationships.

394 Soil and water conservation measures, such as the construction of the check dams  
395 and afforestation, have been undertaken since the 1960s. The areas of two soil and water  
396 conservation measures are plotted in Fig. 5(e), the data of which were collected from  
397 Zhang et al. (2002). The areas of tree planting have an increasing trend, but the slope  
398 gets much larger after 1972. It indicates that greater efforts have been made for  
399 afforestation since the turning point. Similarly, the areas of dammed lands also increase,



400 but the rate gets slower after 1972. These two soil and water conservation measures had  
401 changed the underlying surface of the watershed and impacted the relationship between  
402 precipitation and runoff (Gao et al., 2017; Jiao et al., 2017).

### 403 **3.3 Study area: Xun River basin**

404 The proposed method was also applied to the Xun River basin, China (Fig. 5(b)).  
405 Located between 108°24'–109°26' E and 32°52'–33°55' N, the study area covers  
406 approximately 6448 km<sup>2</sup>. The Xun River is ~218 km long and has an average annual  
407 flow of 73 m<sup>3</sup>/s (Li et al., 2016). The basin has a subtropical monsoon climate. The  
408 weather is wet and moderate with an annual average temperature of 15–17 °C. The daily  
409 hydrological data from 1991–2001 include precipitation from 28 rainfall stations, pan  
410 evaporation from three hydrological gauged stations, and discharge at the outlet of the  
411 Xun River basin. Areal precipitation was obtained using the Thiessen polygon method,  
412 and areal pan evaporation was computed using the average value of the data from  
413 gauged stations. The data in the Xun River basin were also obtained from the local  
414 Hydrology and Water Resources Bureau of China, and there are no gaps among these  
415 data for all the hydrological stations.

416 It can be observed from Fig. 5(d) that no trend is found in annual precipitation,  
417 pan evaporation and streamflow, suggesting that the relationship between precipitation  
418 and runoff of the Xun River basin is rarely affected by human activities during 1991-  
419 2001. However, there exhibit strong seasonal patterns in these three climatic and  
420 hydrological variables, suggesting that seasonal variations in hydrological parameters

421 should be considered.

## 422 **4. Results**

### 423 **4.1 Synthetic experiment**

#### 424 **4.1.1 Results of synthetic experiment with the TMWB model**

425 When using SSC-DP, the first task is to define how the hydrological data series  
426 should be split into the  $k$  sub-periods within which the parameters are assumed to be  
427 constant. As climate change can induce seasonal or half-annual variations while human  
428 activities usually influence the watershed annually, lengths of three months, six months,  
429 and 12 months were arbitrarily chosen. Thus, this experiment compared the following  
430 four methods: (1) EnKF; (2) 3-SSC-DP; (3) 6-SSC-DP, and (4) 12-SSC-DP.

431 Figure 6(a) presents the runoff simulation performance for various scenarios. In  
432 scenario 1, the NSE values of the three SSC-DP methods are all higher than that of  
433 EnKF. The results of  $NSE_{in}$  show no significant differences among various methods.  
434 For scenarios 2, 4, and 6, where true parameters have linear trends, the 6-SSC-DP and  
435 12-SSC-DP are superior to the EnKF and 3-SSC-DP in terms of NSE and  $NSE_{in}$ . In  
436 scenario3, where the true parameters have periodic variations and change every month,  
437 the NSE and  $NSE_{in}$  values of 6-SSC-DP and 12-SSC-DP decrease significantly,  
438 because the assumed sub-period length is longer than the time-scale of actual variations.  
439 Similarly, in scenario 5, 12-SSC-DP performs worst for NSE and  $NSE_{in}$ , but 6-SSC-  
440 DP performs best. In scenario 7 and 8, both 6-SSC-DP and 12-SSC-DP perform better  
441 than EnKF. According to the evaluations of NSE and  $NSE_{in}$ , the SSC-DP offers

442 improved accuracy than the EnKF if the proper length is chosen. Another advantage of  
443 the SSC-DP is the small RE. For all scenarios, the SSC-DP methods significantly  
444 outperform for RE compared with EnKF. Among the SSC-DP methods, the RE of 3-  
445 SSC-DP is the smallest.

446 Figures 6 (b) and (c) focuses on the ability of the four methods to identify time-  
447 varying parameters. It can be seen that the RMSE and MARE values of the 3-SSC-DP  
448 are larger than those of other methods in most cases. That is because the sub-period  
449 length that serves as a calibration period for MCMC is too short (i.e., three months) that  
450 the estimated parameters are associated with higher uncertainties.

451 Regarding the synthetic true parameters are constant values (scenario 1), 12-SSC-  
452 DP gives the best performance with the lowest RMSE, MARE and highest  $R^2$ . The  
453 observations and estimated parameters are presented in Figure 7 (b). It shows that the  
454 estimated parameters obtained by EnKF vary at every time step, resulting in larger  
455 deviations from the observations than 6-SSC-DP and 12-SSC-DP.

456 When the synthetic true parameters vary linearly (scenarios 2, 4, and 6), 12-SSC-  
457 DP produces the best estimations in comparison with EnKF, 3-SSC-DP, and 6-SSC-  
458 DP. The performances of 6-SSC-DP and EnKF are similar.

459 When the synthetic true parameters vary sinusoidally from month to month, EnKF  
460 gives the best estimations in scenario 3. The poor performances of 6-SSC-DP and 12-  
461 SSC-DP can be explained by the sub-period length being much longer than the actual  
462 one. When the parameters vary periodically at six-month intervals (scenario 5), 6-SSC-  
463 DP yields the best performance with the lowest RMSE, MARE and highest  $R^2$ . The

464 differences in estimation performances among 3-SSC-DP, 12-SSC-DP and EnKF are  
465 small. The estimated parameters for scenario 5 have been plotted in Fig. 7(a). Although  
466 3-SSC-DP and 12-SSC-DP have different lengths of sub-periods, they can also detect  
467 the correct seasonal signal of the parameters. For the annual variation in parameters  
468 (scenario 7), 12-SSC-DP and 6-SSC-DP produce better results than EnKF. Similar  
469 results can be seen in scenario 8 where  $C$  has a combined variation from year to year.  
470 In summary, the results indicate that the SSC-DP with a suitable length can estimate  
471 more accurate parameters than EnKF.

#### 472 **4.1.2 Results of synthetic experiment with the Xinanjiang model**

473 The Xinanjiang model is more complex than TMWB, and so some sensitivity  
474 analysis is necessary. As stated in Sect. 3.1.2, the sensitive parameters are  $KE$ ,  $CI$ ,  $CG$ ,  
475  $KI$ ,  $KG$ , and  $NK$ . The 18000 hourly hydrological data points were divided into 25 sub-  
476 periods (monthly time scale) and 12 sub-periods (bimonthly time scale). It is considered  
477 that a monthly time scale helps diagnose seasonal variations, whereas a two-monthly  
478 time scale provides data for longer calibration lengths.

479 Three data assimilation methods (see Sect. 2.3.2 for details) were applied to the  
480 synthetic data: (1) EnKF; (2) EnKS, and (3) SSC-EnKF. The results in Fig. 8 indicate  
481 that EnKS is superior to EnKF, as previously observed (Li et al., 2013), although SSC-  
482 EnKF gives the best results. This is probably because SSC-EnKF is based on the  
483 assumption that the parameters remain constant during each sub-period.

484 The simulated streamflow and identification of time-varying parameters were

485 compared across four methods: 1-SSC, SSC-EnKF, 1-SSC-DP, and 2-SSC-DP. The  
486 simulation performance is summarized in Figure 9(a). For all scenarios, the NSE of 2-  
487 SSC-DP is the lowest, but it performs better for low flows. The SSC-EnKF produces  
488 the highest RE in scenarios 2, 3 and 4, indicating the problem of simulating water  
489 balance. The SSC and 1-SSC-DP perform well for all scenarios in terms of NSE, RE  
490 and  $NSE_{in}$ . Wherein, the SSC performs better than the 1-SSC-DP with regard to RE,  
491 while 1-SSC-DP is slightly superior to SSC in scenario 3 with higher  $NSE_{in}$ .

492 Figures 9(b) and (c) compare the time-varying parameter estimation performance  
493 among the four methods. In scenarios 1 and 2, 2-SSC-DP produces the lowest RMSE,  
494 MARE and  $R^2$ , followed by the 1-SSC-DP. The 1-SSC-DP is slightly superior to the 1-  
495 SSC and significantly outperforms the SSC-EnKF for the two scenarios.

496 When the synthetic true parameters vary sinusoidally from month to month  
497 (scenario 3), the estimated parameters are plotted in Fig. 10. It can be seen that 1-SSC-  
498 DP successfully detects a seasonal signal in every parameter. The SSC-EnKF performs  
499 well for  $R^2$ , but it has high MARE. Although the average MARE of the SSC and 2-  
500 SSC-DP are lower than that of SSC-EnKF, the  $R^2$  of them are relatively low. Therein,  
501 from Fig. 10, the estimated parameters by the 1-SSC fluctuate generally periodically,  
502 but the variations are dramatic, resulting in the lowest  $R^2$  for CI, KI, KG and NK. The  
503 estimated parameters of the 2-SSC-DP fluctuate more slowly, but the sub-period length  
504 is too long. In scenario 4, 1-SSC performs better than the SSC-EnKF and 2-SSC-DP,  
505 but is still slightly inferior to the 1-SSC-DP. Overall, the 1-SSC-DP achieves higher-  
506 quality and more robust parameter estimations performances than the other methods.

507 **4.2 Case study: Wuding River basin**

508        Figures 11(a) and (b) show the double mass curves between daily runoff and  
509 precipitation for the Wuding River basin. Similar to the work of Deng et al. (2016), the  
510 two linear slopes ( $p$ -value  $< 0.05$ ) of the curves are different before and after 1972,  
511 demonstrating the relationship between precipitation and runoff changes under the soil  
512 and water conservation measures. This suggests that there are annual variations in the  
513 watershed characteristics. Hence, the length of each sub-period was set to 12 months,  
514 and the time-varying parameters were identified using 12-SSC-DP. Based on daily  
515 Wuding data from 1958–2000, sensitivity analysis showed that nine parameters of the  
516 Xinanjiang model are relatively sensitive:  $WM$ ,  $WUM$ ,  $WLM$ ,  $KE$ ,  $IMP$ ,  $KI$ ,  $KG$ ,  $N$ , and  
517  $NK$ .

518        The simulation results given by 12-SSC-DP were benchmarked against those from  
519 12-SSC, data assimilation, and the conventional method in which all Xinanjiang model  
520 parameters remain constant. The simulation performance is presented in Figure 12. The  
521 values of the NSEs are relatively low, because the streamflow in dry regions is difficult  
522 to simulate. It can be seen that the 12-SSC-DP gives the best simulation results among  
523 different methods with the highest NSE,  $NSE_{in}$  and small RE. Although the 12-SSC  
524 produces relatively high NSE, it performs the worst simulations for low flows. The  
525 SSC-EnKF has relatively high  $NSE_{in}$ , but the RE of it is the largest. Overall, the 12-  
526 SSC-DP significantly improves the simulation performance of the Xinanjiang model in  
527 the Wuding River basin.

528        Although the objective function of 12-SSC-DP considers the trade-off between

529 simulation accuracy and parameter continuity, 12-SSC-DP gives a higher NSE value.  
530 This may be because 12-SSC locates a local peak over one sub-period, resulting in  
531 unreasonable model states for the beginning of the next sub-period, whereas 12-SSC-  
532 DP uses dynamic programming to explore more reasonable parameter values and model  
533 states. Figure 13 shows the quantile-quantile plots, from which it can be seen that if the  
534 parameters are assumed to be constant, streamflow is highly underestimated. The  
535 underestimation mainly derives from the deficiencies of the model structure. Methods  
536 12-SSC and 12-SSC-DP reduce this underestimation by using time-varying parameters.  
537 Additionally, 12-SSC-DP is slightly inferior to 12-SSC in terms of peak flows, but is  
538 superior in terms of simulating streamflow lower than  $100 \text{ m}^3/\text{s}$ , which accounts for 80 %  
539 of the whole streamflow time series. It can be inferred that the 12-SSC-DP is more  
540 applicable to the simulation of streamflow in the Wuding River basin.

541 The estimated time-varying parameters estimated by 12-SSC-DP are plotted in  
542 Fig.14. The results show that  $WM$  remains constant before and after 1972, but  $WUM$   
543 varies significantly over this period, indicating that the distribution of soil water  
544 capacity may change, i.e.,  $WUM$  decreases but  $WLM$  increases. A Person correlation  
545 analysis is applied to investigate the relationship between the areas of tree planting and  
546  $WUM$  as well as  $WLM$ . It is found that there is a significant negative correlation  
547 (Pearson correlation efficient  $\rho=-0.38$ ,  $P<0.05$ ) between the areas of tree planting and  
548  $WUM$ . While  $WLM$  has a nonsignificant positive correlation ( $\rho=0.26$ ,  $P>0.05$ ) with the  
549 areas of tree planting. It can be inferred that less severe soil erosion occurred, because  
550 the upper layers became thinner while the lower layer, where vegetation roots dominate,

551 became thicker (Jayawardena and Zhou, 2000). Additionally, *IMP* is significantly  
552 correlated with the areas of tree planting ( $\rho=-0.33$ ,  $P<0.05$ ). Except for afforestation,  
553 the areas of the dammed lands are significantly correlated with *WLM* ( $\rho=0.46$ ,  $P<0.05$ ),  
554 suggesting that the construction of the check dams also has an influence on the soil  
555 water capacity of the Wuding river basin. Other parameters, *KE*, *KI*, *KG*, *N* and *NK*  
556 have little differences before and after 1972. The variations in *WLM* and *IMP* slowed  
557 down after the turning point, similar to the results of Deng et al. (2016).

#### 558 4.3 Case study: Xun River basin

559 Figures 11(c) and (d) show the double mass curves between runoff and  
560 precipitation for the Xun River basin. The linear slope of the curve is generally  
561 stationary for the whole ten-year period shown in Fig. 11(c), with a correlation  
562 coefficient of 99.6 %. In contrast, the linear slope for an intra-annual timescale is non-  
563 stationary (Fig. 11(d)). Based on these results, it can be inferred that the relationship  
564 between precipitation and runoff is stable from 1990–2000, but varies over the intra-  
565 annual timescale. Hence, sub-periods of three and 12 months were examined in the Xun  
566 River basin using models 3-SSC-DP and 12-SSC-DP. From the Xun River basin data  
567 from 1991–2000, sensitivity analysis suggested that five parameters of the Xinanjiang  
568 model are relatively sensitive, namely *KE*, *B*, *KI*, *KG*, and *NK*.

569 Similar to the case study of the Wuding River basin, the simulation performance  
570 of 3-SSC-DP was benchmarked against that of 3-SSC, data assimilation, and the  
571 conventional calibration method. Among the data assimilation methods described in



572 Sect. 2.3.2, 3-SSC-EnKF gives the highest simulation accuracy. The simulation  
573 performance is presented in Figure 15. All methods performed well, with NSE values  
574 of 92.5 %, 93.0 %, 95.0 %, and 94.8 % for the conventional method, 3-SSC-EnKF, 3-  
575 SSC, and 3-SSC-DP, respectively. 3-SSC and 3-SSC-DP also perform well for  $NSE_m$   
576 compared with 3-SSC-EnKF and the conventional method. However, as regards to RE,  
577 the values are 0.0007 and 0.0324 for 3-SSC-DP and 3-SSC-DP, respectively. It  
578 indicated that the 3-SSC-DP can better simulate water balance than the 3-SSC in the  
579 Xun River basin. Figure 16 illustrates the hydrograph and quantile-quantile plots for  
580 the simulations in the Xun river basin. It is evident that the peak flows estimated by the  
581 3-SSC are higher than those of 3-SSC-DP, and 3-SSC-DP simulate better the flows  
582 ranging from  $100 \text{ m}^3/\text{s}$  to  $200 \text{ m}^3/\text{s}$ .

583 The estimated parameters using 3-SSC-DP are presented in Fig. 17(a). Some  
584 parameters vary significantly over an intra-annual time scale. Among them, the  
585 parameter  $KE$ , representing the ratio of potential evapotranspiration to pan evaporation,  
586 exhibits the most distinct seasonal variations. A fast Fourier transform was used to  
587 calculate the spectral power of the  $KE$  time series to explore its periodic characteristics.  
588 As can be observed from Fig. 17(b), 3-SSC-DP had the greatest spectral power, for a  
589 period of 4.0 cycles per year, somewhat higher than the power obtained by 3-SSC and  
590 3-SSC-EnKF. This means a stronger periodic pattern is captured by 12-SSC-DP. Given  
591 that the estimated  $KE$  varies at three-monthly intervals, it has a one-year periodicity.  
592 The other parameters do not exhibit significant one-year periodic patterns. This may be  
593 because only  $KE$ , linking potential evapotranspiration and pan evaporation, is directly

594 impacted by seasonal climate variations, such as temperature.

## 595 **5. Discussion**

596 As noted in the methodology section, the performance of the proposed method is  
597 influenced by several factors, such as the weights in the objective function and the  
598 choice of lengths. Some suggestions regarding the improvement of the proposed  
599 approach are now discussed in detail.

### 600 **5.1 Objective function of dynamic programming in SSC-DP**

601 In the conventional method, a parameter set is identified as optimal for providing  
602 the best simulation over the calibration period. However, other parameter sets with  
603 slightly worse (but still good) performance can also be candidates. Allowing for input  
604 data uncertainty and local optima, SSC-DP identifies parameter sets that perform near-  
605 optimally and display fewer fluctuations over sub-periods. This can be adjusted by  
606 weights in the objective function of the dynamic programming approach (see Eq. (3)).  
607 As the weighting for accuracy increases, parameters providing more accurate  
608 simulations are chosen, but parameter continuity is less important. If too much  
609 importance is given to continuity, the variations in real-world processes may be  
610 underestimated. Here, the influence of different weights has been assessed for  
611 simulation accuracy and parameter continuity based on synthetic experiments with the  
612 TMWB and Xinanjiang models, respectively. Specifically, the weight for simulation  
613 accuracy was set to 1, and the weight for parameter continuity  $\alpha$  varied from zero to a  
614 small positive value (e.g., 1). When  $\alpha = 0$ , only simulation accuracy was considered.

615 Figure 18(a) shows the  $R^2$  value of 12-SSC-DP with various continuity weights for  
616 scenario 4 in the synthetic experiment with the TMWB model. It can be seen that  $R^2$  is  
617 lowest when  $\alpha = 0$  for both  $C$  and  $SC$ . There is some improvement when a nonzero  
618 weight is applied. As  $\alpha$  increases, the performance of 12-SSC-DP improves, and then  
619 worsens; the differences among schemes with nonzero weights are not distinct. Similar  
620 results can be observed in Fig. 18(b), which presents the  $R^2$  value of 12-SSC-DP with  
621 various  $\alpha$  for scenario 2 in the synthetic experiment with the Xinanjiang model.  
622 Therefore, nonzero continuity weights can significantly improve the parameter  
623 estimation performance compared with the zero-weight case. It is suggested that  
624 weights of 1 (accuracy) and 0.005 (continuity) be used with the TMWB model and  
625 weights of 1 (accuracy) and 0.2 (continuity) be applied with the Xinanjiang model, as  
626 in this study.

## 627 5.2 Choice of sub-period length in SSC-DP

628 As mentioned by Gharari et al. (2013), there are different ways of determining the  
629 sub-period lengths. The sub-periods can be non-continuous hydrological years (Seiller  
630 et al., 2012), months or seasons (Deng et al., 2018; Paik et al., 2005), and discharge or  
631 precipitation events (Singh and Bardossy, 2012). This introduces a controversial issue  
632 whereby parameters are impacted by the length of the calibration period. Merz et al.  
633 (2009) suggested that 3–5 years is an acceptable calibration period, whereas Singh and  
634 Bardossy (2012) indicated that a small number of events may be sufficient for  
635 parameter identification. It is suggested that the determination of the sub-period length

636 considers three factors:

637 (1) The temporal scale of climate change or human activities. For example, the  
638 Wudinghe River basin is taken as a case study. The soil and water conservation  
639 measures have led to a durative and long-term change in the catchment characteristic  
640 since the 1960s. Due to this, the yearly sub-period is preferred.

641 (2) The seasonality. Contrary to the Wudinghe River basin, the relationship  
642 between precipitation and runoff of the Xun River basin is rarely affected by human  
643 activities during 1991-2001. However, its significant seasonal dynamics can be  
644 observed and has been studied in the literature (Lan et al., 2020; Lan et al., 2018). In  
645 order to diagnose the seasonality, the stable period of 3-month is adopted.

646 (3) The simulation accuracy. The length should be neither too long nor too short  
647 so as to increase the reliability of the calibration while guaranteeing that variations in  
648 real processes are captured. Thus, given that the time scale of the variations is unknown,  
649 the proposed SSC-DP can be used with different split-sample lengths. It is suggested  
650 that the length should be as long as possible without degrading the simulation  
651 performance significantly. For example, in the synthetic experiment with the TMWB  
652 model, if the difference between the NSE values of 6-SSC-DP and 3-SSC-DP is small,  
653 the preferred length is 6-month.

654 However, many studies are based on the conventional assumption that the  
655 parameters of different sub-periods are independent. Hence, the sub-period lengths  
656 should be long enough to reduce the degree of uncertainty. In this study, the assumption  
657 of parameter continuity is introduced to give another constraint that considers

658 correlations between parameters of adjacent sub-periods. It appears that the  
659 determination of sub-period lengths deserves further investigation.

## 660 **6. Conclusions**

661 This paper has described a time-varying parameter estimation approach based on  
662 dynamic programming. The proposed SSC-DP combines the basic concept of SSC and  
663 the continuity assumption of data assimilation to estimate more continuous parameters  
664 while providing comparably good streamflow simulations. Two synthetic experiments  
665 were designed to evaluate its applicability and efficiency for time-varying parameter  
666 identification. Furthermore, two case studies were conducted to explore the advantages  
667 of SSC-DP in real catchments. From the results, the following conclusions can be drawn:

668 1. The proposed method with a suitable length not only produces better simulation  
669 performance, but also ensures more accurate parameter estimates than SSC and EnKF  
670 in the synthetic experiment using the TMWB model with two parameters. The impact  
671 of sub-period lengths on the performance of SSC-DP is significant when the pre-  
672 determined parameters vary sinusoidally.

673 2. The proposed method can be used to deal with complex hydrological models  
674 involving a large number of parameters, demonstrated by the synthetic experiment  
675 using the Xinanjiang model with 15 parameters. A sensitivity analysis was performed  
676 to reduce the probable computational cost and improve the efficiency of identifying the  
677 time-varying parameters.

678 3. The proposed method has the potential to detect the relationship between the  
679 time-varying parameters and dynamic catchment characteristics. For example, SSC-DP

680 produces the best simulation performance in the case study of the Wuding River basin  
681 and detects that parameters representing soil water capacity and impervious areas  
682 changed significantly after 1972, reflecting the soil and water conservation projects  
683 carried out from 1958–2000. Additionally, SSC-DP detects the strongest seasonal signal  
684 in the case study of Xun River basin, indicating the distinct impacts of seasonal climate  
685 variability.

686 This study has demonstrated that the proposed method is an effective approach for  
687 identifying time-varying parameters under changing environments. Further work is still  
688 needed, such as to determine an objective method for choosing the sub-period lengths.

#### 689 **Acknowledgements**

690 This study was supported by the Natural Science Foundation of Hubei Province  
691 (2017CFA015), the National Natural Science Foundation of China (51861125102), and  
692 Innovation Team in Key Field of the Ministry of Science and Technology  
693 (2018RA4014). The authors would like to thank the editor and anonymous reviewers  
694 for their comments that helped improve the quality of the paper.

695

#### 696 **Code/Data availability**

697 The data and codes that support the findings of this study are available from the  
698 corresponding author upon request.

699

700 **Author contribution**

701 All of the authors helped to develop the method, designed the experiments, analyzed  
702 the results and wrote the paper.

703

704 **Compliance with Ethical Standards**

705 **Conflict of Interest** The authors declare that they have no conflict of interest.

706

707

708 **References**

- 709 Alvisi, S., Mascellani, G., Franchini, M., Bardossy, A., 2006. Water level forecasting through fuzzy logic  
710 and artificial neural network approaches. *Hydrology and Earth System Sciences* 10(1), 1-17.
- 711 Bellman, R., 1957. *Dynamic programming*. Princeton University Press, Princeton.
- 712 Broderick, C., Matthews, T., Wilby, R.L., Bastola, S., Murphy, C., 2016. Transferability of hydrological  
713 models and ensemble averaging methods between contrasting climatic periods. *Water*  
714 *Resources Research* 52(10), 8343-8373.
- 715 Bronstert, A., 2004. Rainfall-runoff modelling for assessing impacts of climate and land-use change.  
716 *Hydrological Processes* 18(3), 567-570.
- 717 Chen, Y., Zhang, D., 2006. Data assimilation for transient flow in geologic formations via ensemble  
718 kalman filter. *Advances in Water Resources* 29(8), 1107-1122.
- 719 Chib, S., Greenberg, E., 1995. Understanding the metropolis-hastings algorithm. *American Statistician*  
720 49(4), 327-335.
- 721 Coron, L. et al., 2012. Crash testing hydrological models in contrasted climate conditions: An experiment  
722 on 216 australian catchments. *Water Resources Research* 48.
- 723 Dai, C., Qin, X.S., Chen, Y., Guo, H.C., 2018. Dealing with equality and benefit for water allocation in a  
724 lake watershed: A gini-coefficient based stochastic optimization approach. *Journal of*  
725 *Hydrology* 561, 322-334.
- 726 Dawson, C.W., Abrahart, R.J., See, L.M., 2007. Hydrotest: A web-based toolbox of evaluation metrics for  
727 the standardised assessment of hydrological forecasts. *Environmental Modelling & Software*  
728 22(7), 1034-1052.
- 729 Deng, C., Liu, P., Guo, S., Li, Z., Wang, D., 2016. Identification of hydrological model parameter variation  
730 using ensemble kalman filter. *Hydrology and Earth System Sciences* 20(12), 4949-4961.
- 731 Deng, C., Liu, P., Wang, D., Wang, W., 2018. Temporal variation and scaling of parameters for a monthly  
732 hydrologic model. *Journal of Hydrology* 558, 290-300.
- 733 Deng, C., Liu, P., Wang, W., Shao, Q., Wang, D., 2019. Modelling time-variant parameters of a two-  
734 parameter monthly water balance model. *Journal of Hydrology* 573, 918-936.
- 735 Duan, Q. et al., 2006. Model parameter estimation experiment (mopex): An overview of science strategy

736 and major results from the second and third workshops. *Journal of Hydrology* 320(1-2), 3-17.

737 Feng, M. et al., 2017. Deriving adaptive operating rules of hydropower reservoirs using time-varying  
738 parameters generated by the enkf. *Water Resources Research* 53(8), 6885-6907.

739 Fowler, K., Peel, M., Western, A., Zhang, L., 2018. Improved rainfall-runoff calibration for drying climate:  
740 Choice of objective function. *Water Resources Research* 54(5), 3392-3408.

741 Fowler, K.J.A., Peel, M.C., Western, A.W., Zhang, L., Peterson, T.J., 2016. Simulating runoff under  
742 changing climatic conditions: Revisiting an apparent deficiency of conceptual rainfall-runoff  
743 models. *Water Resources Research* 52(3), 1820-1846.

744 Gao, S. et al., 2017. Derivation of low flow frequency distributions under human activities and its  
745 implications. *Journal of Hydrology* 549, 294-300.

746 Gharari, S., Hrachowitz, M., Fenicia, F., Savenije, H.H.G., 2013. An approach to identify time consistent  
747 model parameters: Sub-period calibration. *Hydrology and Earth System Sciences* 17(1), 149-  
748 161.

749 Guo, S.L., Wang, J.X., Xiong, L.H., Ying, A.W., Li, D.F., 2002. A macro-scale and semi-distributed monthly  
750 water balance model to predict climate change impacts in china. *Journal of Hydrology* 268(1-  
751 4), 1-15.

752 Guzha, A.C., Rufino, M.C., Okoth, S., Jacobs, S., Nobrega, R.L.B., 2018. Impacts of land use and land cover  
753 change on surface runoff, discharge and low flows: Evidence from east africa. *Journal of*  
754 *Hydrology-Regional Studies* 15, 49-67.

755 Hock, R., 1999. A distributed temperature-index ice- and snowmelt model including potential direct  
756 solar radiation. *Journal of Glaciology* 45(149), 101-111.

757 Hughes, D.A., 2015. Simulating temporal variability in catchment response using a monthly rainfall-  
758 runoff model. *Hydrological Sciences Journal-Journal Des Sciences Hydrologiques* 60(7-8), 1286-  
759 1298.

760 Hundecha, Y., Bardossy, A., 2004. Modeling of the effect of land use changes on the runoff generation  
761 of a river basin through parameter regionalization of a watershed model. *Journal of Hydrology*  
762 292(1-4), 281-295.

763 Jayawardena, A.W., Zhou, M.C., 2000. A modified spatial soil moisture storage capacity distribution  
764 curve for the xinanjiang model. *Journal of Hydrology* 227(1-4), 93-113.

765 Jeremiah, E., Marshall, L., Sisson, S.A., Sharma, A., 2013. Specifying a hierarchical mixture of experts for  
766 hydrologic modeling: Gating function variable selection. *Water Resources Research* 49(5),  
767 2926-2939.

768 Jiao, Y. et al., 2017. Impact of vegetation dynamics on hydrological processes in a semi-arid basin by  
769 using a land surface-hydrology coupled model. *Journal of Hydrology* 551, 116-131.

770 Jie, M.X. et al., 2018. Transferability of conceptual hydrological models across temporal resolutions:  
771 Approach and application. *Water Resources Management* 32(4), 1367-1381.

772 Khalil, M., Panu, U.S., Lennox, W.C., 2001. Groups and neural networks based streamflow data infilling  
773 procedures. *Journal of Hydrology* 241(3-4), 153-176.

774 Kim, S., Hong, S.J., Kang, N., Noh, H.S., Kim, H.S., 2016. A comparative study on a simple two-parameter  
775 monthly water balance model and the kajiyama formula for monthly runoff estimation.  
776 *Hydrological Sciences Journal-Journal Des Sciences Hydrologiques* 61(7), 1244-1252.

777 Kim, S.M., Benham, B.L., Brannan, K.M., Zeckoski, R.W., Doherty, J., 2007. Comparison of hydrologic  
778 calibration of hspf using automatic and manual methods. *Water Resources Research* 43(1).

779 Kim, S.S.H., Hughes, J.D., Chen, J., Dutta, D., Vaze, J., 2015. Determining probability distributions of



780 parameter performances for time-series model calibration: A river system trial. *Journal of*  
781 *Hydrology* 530, 361-371.

782 King, D.M., Perera, B.J.C., 2013. Morris method of sensitivity analysis applied to assess the importance  
783 of input variables on urban water supply yield - a case study. *Journal of Hydrology* 477, 17-32.

784 Klemes, V., 1986. Operational testing of hydrological simulation-models. *Hydrological Sciences Journal-*  
785 *Journal Des Sciences Hydrologiques* 31(1), 13-24.

786 Lan, T., Lin, K., Xu, C.-Y., Tan, X., Chen, X., 2020. Dynamics of hydrological-model parameters:  
787 Mechanisms, problems and solutions. *Hydrology and Earth System Sciences* 24(3), 1347-1366.

788 Lan, T. et al., 2018. A clustering preprocessing framework for the subannual calibration of a hydrological  
789 model considering climate-land surface variations. *Water Resources Research* 54(0).

790 Li, H. et al., 2018. Hybrid two-stage stochastic methods using scenario-based forecasts for reservoir refill  
791 operations. *Journal of Water Resources Planning and Management* 144(12).

792 Li, H., Zhang, Y., 2017. Regionalising' rainfall-runoff modelling for predicting daily runoff: Comparing  
793 gridded spatial proximity and gridded integrated similarity approaches against their lumped  
794 counterparts. *Journal of Hydrology* 550, 279-293.

795 Li, Y., Ryu, D., Western, A.W., Wang, Q.J., 2013. Assimilation of stream discharge for flood forecasting:  
796 The benefits of accounting for routing time lags. *Water Resources Research* 49(4), 1887-1900.

797 Li, Z. et al., 2016. Evaluation of estimation of distribution algorithm to calibrate computationally  
798 intensive hydrologic model. *Journal of Hydrologic Engineering* 21(6).

799 Lin, K. et al., 2014. Xinjiang model combined with curve number to simulate the effect of land use  
800 change on environmental flow. *Journal of Hydrology* 519, 3142-3152.

801 Lu, H. et al., 2013. The streamflow estimation using the xinjiang rainfall runoff model and dual state-  
802 parameter estimation method. *Journal of Hydrology* 480, 102-114.

803 Luo, M., Pan, C., Zhan, C., 2019. Diagnosis of change in structural characteristics of streamflow series  
804 based on selection of complexity measurement methods: Fenhe river basin, china. *Journal of*  
805 *Hydrologic Engineering* 24(2).

806 Meng, S., Xie, X., Liang, S., 2017. Assimilation of soil moisture and streamflow observations to improve  
807 flood forecasting with considering runoff routing lags. *Journal of Hydrology* 550, 568-579.

808 Merz, R., Parajka, J., Bloeschl, G., 2009. Scale effects in conceptual hydrological modeling. *Water*  
809 *Resources Research* 45.

810 Merz, R., Parajka, J., Bloeschl, G., 2011. Time stability of catchment model parameters: Implications for  
811 climate impact analyses. *Water resources research* 47(W02531).

812 Ming, B., Liu, P., Bai, T., Tang, R., Feng, M., 2017. Improving optimization efficiency for reservoir  
813 operation using a search space reduction method. *Water Resources Management* 31(4), 1173-  
814 1190.

815 Moradkhani, H., Sorooshian, S., Gupta, H.V., Houser, P.R., 2005. Dual state-parameter estimation of  
816 hydrological models using ensemble kalman filter. *Advances in Water Resources* 28(2), 135-  
817 147.

818 Morris, M.D., 1991. Factorial sampling plans for preliminary computational experiments. *Technometrics*  
819 33(2), 161-174.

820 Nash, J.E., Sutcliffe, J.V., 1970. River flow forecasting through conceptual models part i — a discussion  
821 of principles. *Journal of Hydrology* 10(3), 282-290.

822 Paik, K., Kim, J.H., Kim, H.S., Lee, D.R., 2005. A conceptual rainfall-runoff model considering seasonal  
823 variation. *Hydrological Processes* 19(19), 3837-3850.

824 Pappenberger, F., Beven, K.J., Ratto, M., Matgen, P., 2008. Multi-method global sensitivity analysis of  
825 flood inundation models. *Advances in Water Resources* 31(1), 1-14.

826 Pathiraja, S. et al., 2018. Time-varying parameter models for catchments with land use change: The  
827 importance of model structure. *Hydrology and Earth System Sciences* 22(5), 2903-2919.

828 Pathiraja, S., Marshall, L., Sharma, A., Moradkhani, H., 2016. Hydrologic modeling in dynamic  
829 catchments: A data assimilation approach. *Water Resources Research* 52(5), 3350-3372.

830 Poulin, A., Brissette, F., Leconte, R., Arsenault, R., Malo, J.-S., 2011. Uncertainty of hydrological modelling  
831 in climate change impact studies in a canadian, snow-dominated river basin. *Journal of*  
832 *Hydrology* 409(3-4), 626-636.

833 Quoc Quan, T., De Niel, J., Willems, P., 2018. Spatially distributed conceptual hydrological model building:  
834 A genetic top-down approach starting from lumped models. *Water Resources Research* 54(10),  
835 8064-8085.

836 Rebolho, C., Andreassian, V., Le Moine, N., 2018. Inundation mapping based on reach-scale effective  
837 geometry. *Hydrology and Earth System Sciences* 22(11), 5967-5985.

838 Refsgaard, J.C., Knudsen, J., 1996. Operational validation and intercomparison of different types of  
839 hydrological models. *Water Resources Research* 32(7), 2189-2202.

840 Seiller, G., Anctil, F., Perrin, C., 2012. Multimodel evaluation of twenty lumped hydrological models  
841 under contrasted climate conditions. *Hydrology and Earth System Sciences* 16(4), 1171-1189.

842 Si, W., Bao, W., Gupta, H.V., 2015. Updating real-time flood forecasts via the dynamic system response  
843 curve method. *Water Resources Research* 51(7), 5128-5144.

844 Singh, S.K., Bardossy, A., 2012. Calibration of hydrological models on hydrologically unusual events.  
845 *Advances in Water Resources* 38, 81-91.

846 Siriwardena, L., Finlayson, B.L., McMahon, T.A., 2006. The impact of land use change on catchment  
847 hydrology in large catchments: The comet river, central queensland, australia. *Journal of*  
848 *Hydrology* 326(1-4), 199-214.

849 Sobol, I.M., 1993. Sensitivity estimates for nonlinear mathematical models. *Mathematical modelling*  
850 *and computational experiments* 1(4), 407-414.

851 Stephens, C.M., Marshall, L.A., Johnson, F.M., 2019. Investigating strategies to improve hydrologic  
852 model performance in a changing climate. *Journal of Hydrology* 579.

853 Sun, Y. et al., 2018. Development of multivariable dynamic system response curve method for real-time  
854 flood forecasting correction. *Water Resources Research* 54(7), 4730-4749.

855 Teweldebrhan, A.T., Burkhart, J.F., Schuler, T.V., 2018. Parameter uncertainty analysis for an operational  
856 hydrological model using residual-based and limits of acceptability approaches. *Hydrology and*  
857 *Earth System Sciences* 22(9), 5021-5039.

858 Thirel, G. et al., 2015. Hydrology under change: An evaluation protocol to investigate how hydrological  
859 models deal with changing catchments. *Hydrological Sciences Journal-Journal Des Sciences*  
860 *Hydrologiques* 60(7-8), 1184-1199.

861 Toth, E., Brath, A., 2007. Multistep ahead streamflow forecasting: Role of calibration data in conceptual  
862 and neural network modeling. *Water Resources Research* 43(11).

863 Westra, S., Thyer, M., Leonard, M., Kavetski, D., Lambert, M., 2014. A strategy for diagnosing and  
864 interpreting hydrological model nonstationarity. *Water Resources Research* 50(6), 5090-5113.

865 Xie, S. et al., 2018. A progressive segmented optimization algorithm for calibrating time-variant  
866 parameters of the snowmelt runoff model (srm). *Journal of Hydrology* 566, 470-483.

867 Xiong, L.H., Guo, S.L., 1999. A two-parameter monthly water balance model and its application. *Journal*

868 of Hydrology 216(1-2), 111-123.  
869 Xiong, M. et al., 2019. Identifying time-varying hydrological model parameters to improve simulation  
870 efficiency by the ensemble kalman filter: A joint assimilation of streamflow and actual  
871 evapotranspiration. Journal of Hydrology 568, 758-768.  
872 Xu, J., 2011. Variation in annual runoff of the wudinghe river as influenced by climate change and human  
873 activity. Quaternary International 244(2), 230-237.  
874 Yang, N. et al., 2017. Evaluation of the trmm multisatellite precipitation analysis and its applicability in  
875 supporting reservoir operation and water resources management in hanjiang basin, china.  
876 Journal of Hydrology 549, 313-325.  
877 Yang, X. et al., 2018. A new fully distributed model of nitrate transport and removal at catchment scale.  
878 Water Resources Research 54(8), 5856-5877.  
879 Yin, J. et al., 2018. A copula-based analysis of projected climate changes to bivariate flood quantiles.  
880 Journal of Hydrology 566, 23-42.  
881 Zhang, J., Ji, W., Feng, X., 2002. Water and sediment changes in the wudinghe river: Present state,  
882 formative cause and tendency in the future. A study of water and sediment changes in the  
883 Yellow River 2, 393-429.  
884 Zhao, R.J., 1992. The xinanjiang model applied in china. Journal of Hydrology 135(1-4), 371-381.  
885

Table 1 Parameters of the TMWB model

Parameter	Physical meaning	Range and units
C	Evapotranspiration parameter	0.2-2.0 (-)
SC	Catchment water storage capacity	100-2000 (mm)

Table 2 Parameters of the Xinanjiang model

Category	Parameter	Physical meaning	Range and units
Evapotranspiration	WM	Tension water capacity	80-400 (mm)
	X	$WUM=X \times WM$ , WUM is the tension water capacity of lower layer	0.01-0.8 (-)
	Y	$WLM=Y \times WM$ , WLM is the tension water capacity of deeper layer	0.01-0.8 (-)
	K	Ratio of potential evapotranspiration to pan evaporation	0.4-1.5 (-)
	C	The coefficient of deep evapotranspiration	0.01-0.4 (-)
Runoff production	B	The exponent of the tension water capacity curve	0.1-10 (-)
	IMP	The ratio of the impervious to the total area of the basin	0.01-0.15 (-)
Runoff separation	SM	The areal mean of the free water capacity of the surface soil layer	10-80 (mm)
	EX	The exponent of the free water capacity curve	0.6-6 (-)
	CG	The outflow coefficients of the free water storage to groundwater	0.01-0.45 (-)
	CI	The outflow coefficients of the free water storage to interflow	0.01-0.45 (-)
Flow concentration	N	Number of reservoirs in the instantaneous unit hydrograph	0.5-10 (-)
	NK	Common storage coefficient in the instantaneous unit hydrograph	1-20 (-)
	KG	The recession constant of groundwater storage	0.6-1 (-)
	KI	The recession constant of the lower interflow storage	0.9-1 (-)

Table 3 Different cases of synthetic experiments and real catchment case studies for comparison and evaluation

	Data	Hydrological model	Time-varying parameter estimation methods		
			SSC	SSC- DP	Data assimilation
Synthetic experiment	Monthly synthetic data	TMWB model		✓	✓
	Hourly synthetic data	Xinanjiaing model	✓	✓	✓
Real catchment case study	Daily data from Wuding River basin	Xinanjiaing model	✓	✓	✓
	Daily data from Xun River basin	Xinanjiaing model	✓	✓	✓

Table 4 True parameters of different scenarios in the synthetic experiment with the TMWB model

Scenario	Description
1	Both $C$ and $SC$ are constant
2	Both $C$ and $SC$ have increasing linear trends and change every month
3	Both $C$ and $SC$ have periodic variations and change every month
4	Both $C$ and $SC$ have increasing linear trends and change every six months
5	Both $C$ and $SC$ have periodic variations and change every six months
6	Both $C$ and $SC$ have increasing linear trends and change every year
7	Both $C$ and $SC$ have periodic variations and change every year
8	$C$ has a periodic variation with an increasing linear trend, whereas $SC$ only has an increasing linear trend. The parameters change every year

Table 5 True parameters of different scenarios in the synthetic experiment with the Xinanjiang model

Scenario	Description
1	$KE$ , $CI$ , $CG$ , $KI$ , $KG$ , and $NK$ remain constant
2	$KE$ , $CI$ , $CG$ , $KI$ , $KG$ , and $NK$ have linear trends and change every month
3	$KE$ , $CI$ , $CG$ , $KI$ , $KG$ , and $NK$ have periodic variations and change every month
4	$KE$ has a periodic variation with an increasing linear trend, whereas $CI$ , $CG$ , $KI$ , $KG$ , and $NK$ only have periodic variations. The parameters change every month



**Modeling:**  
Hydrological models and  
sensitivity analysis  
(Section 2.1&2.2)

**Calibration:**  
Time-varying parameter  
estimation method  
(Section 2.3)

**Comparison:**  
Model evaluation criteria  
(Section 2.4)

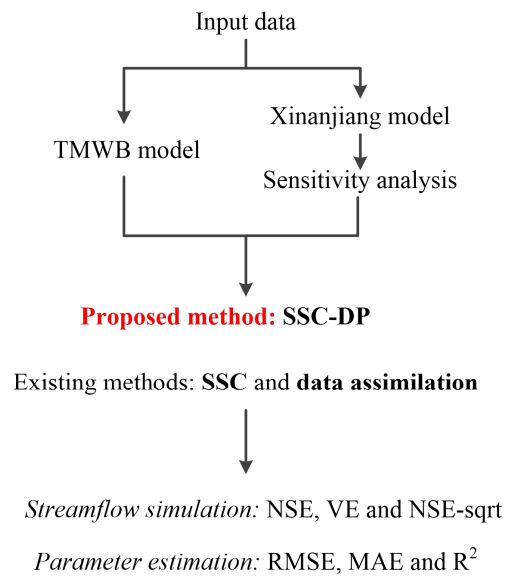


Figure 1 Flowchart of the methodologies

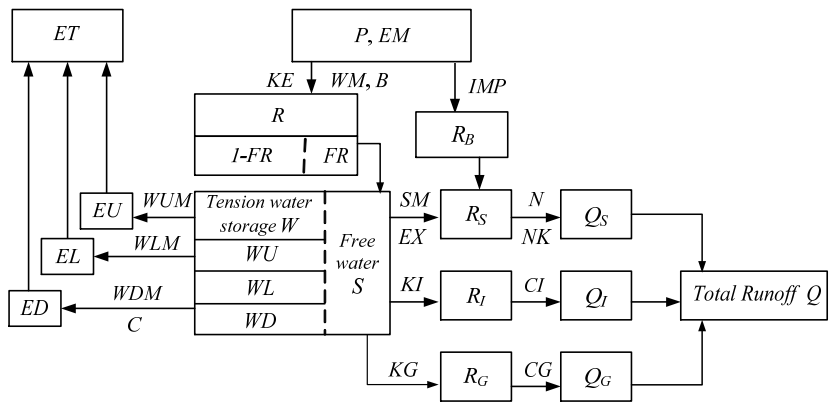


Figure 2 Flowchart of the Xinanjiang model.

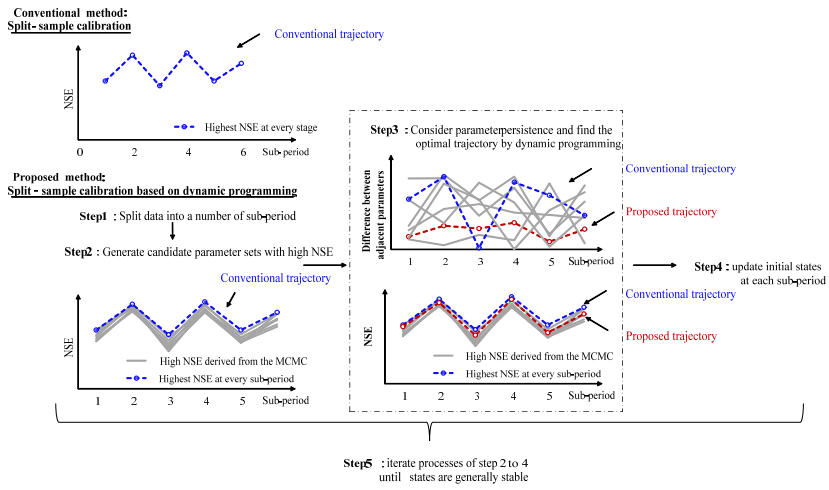


Figure 3 Flowchart of SSC-DP.

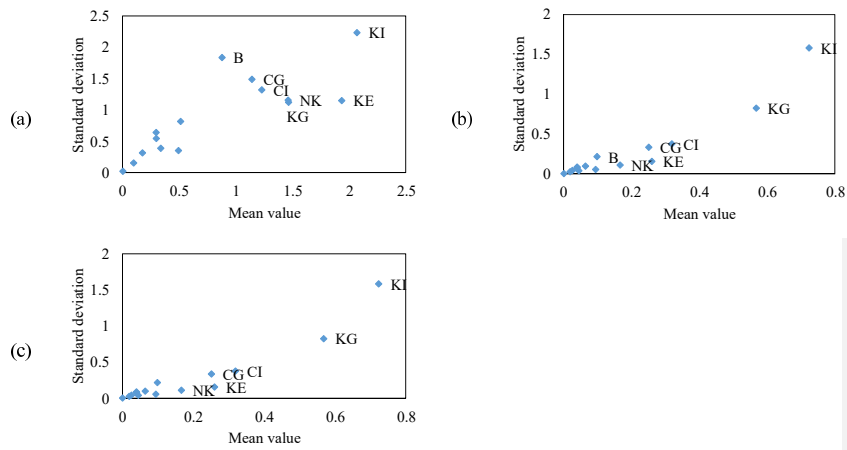


Figure 4 Results of the Morris method for the synthetic experiment with the Xinanjiang model. The sensitivity analysis is based on three different kinds of model responses: (a) NSE; (b)  $NSE_{abs}$ ; (c)  $NSE_{lm}$ . Only the most sensitive parameters are labeled.

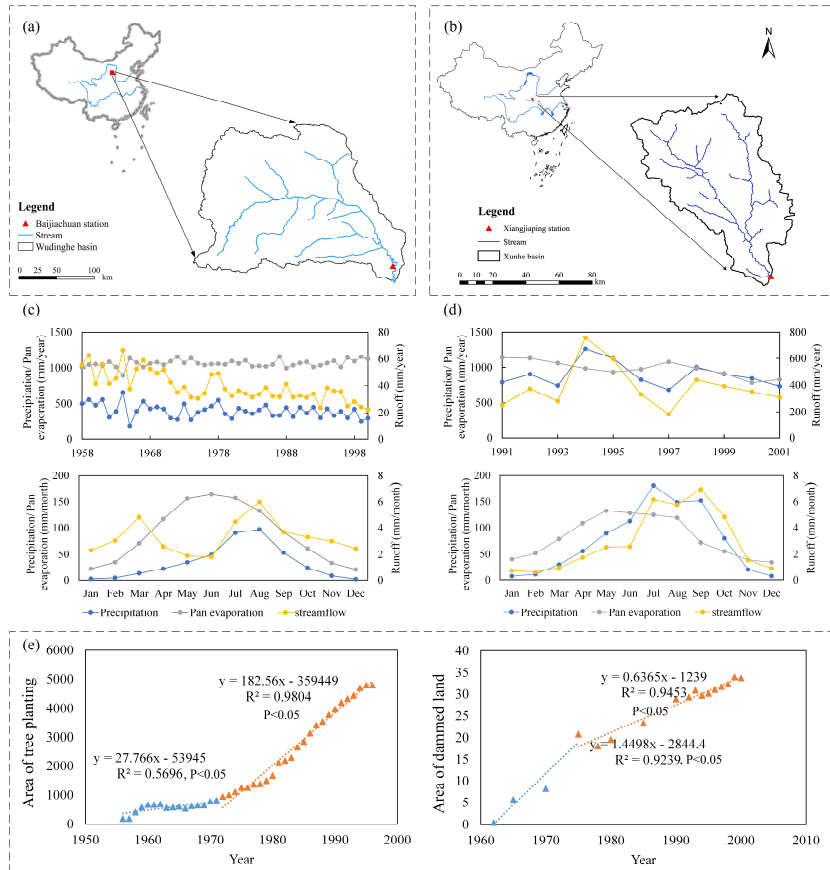
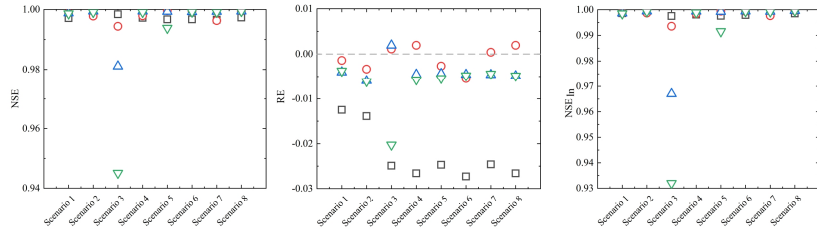
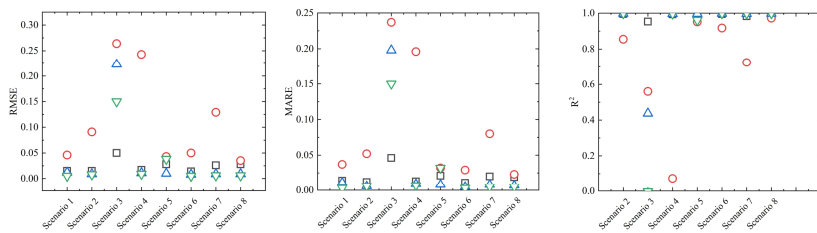


Figure 5 Location of (a) Wuding River basin and (b) Xun River basin. The plots (c) and (d) show the average yearly and monthly variations of precipitation, pan evaporation and streamflow in the Wuding River basin and Xun River basin, respectively. The plot (e) shows the temporal variations in the soil and water conservation measures undertaken in the Wuding River basin.

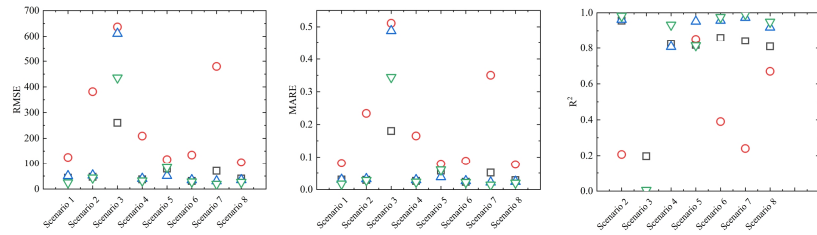
(a) Simulation performance for streamflow



(b) Estimation performance for parameter C



(c) Estimation performance for parameter SC



□ ENKF    ○ 3-SSC-DP    △ 6-SSC-DP    ▽ 12-SSC-DP

Figure 6 Comparison between the EnKF and SSC-DP methods for (a) streamflow simulation and identification of (b) parameter C and (c) parameter SC.

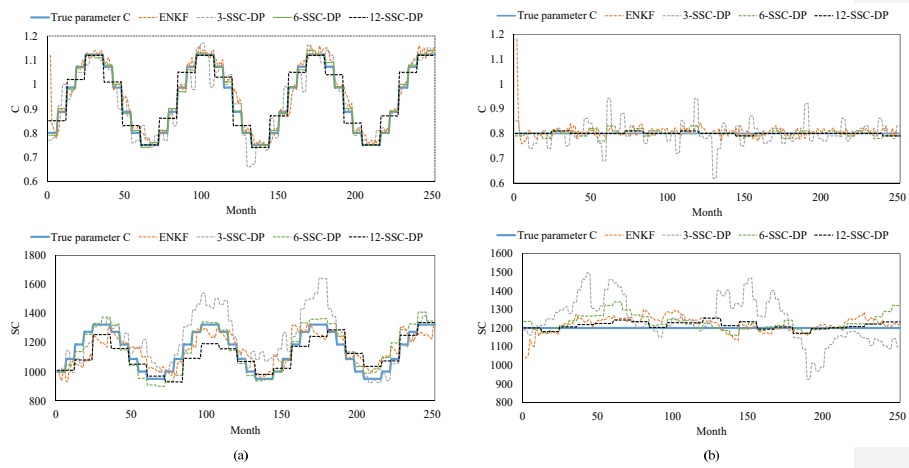


Figure 7 Comparison among different methods for (a) scenario 5 and (b) scenario 1 of the synthetic experiment with the TMWB model.

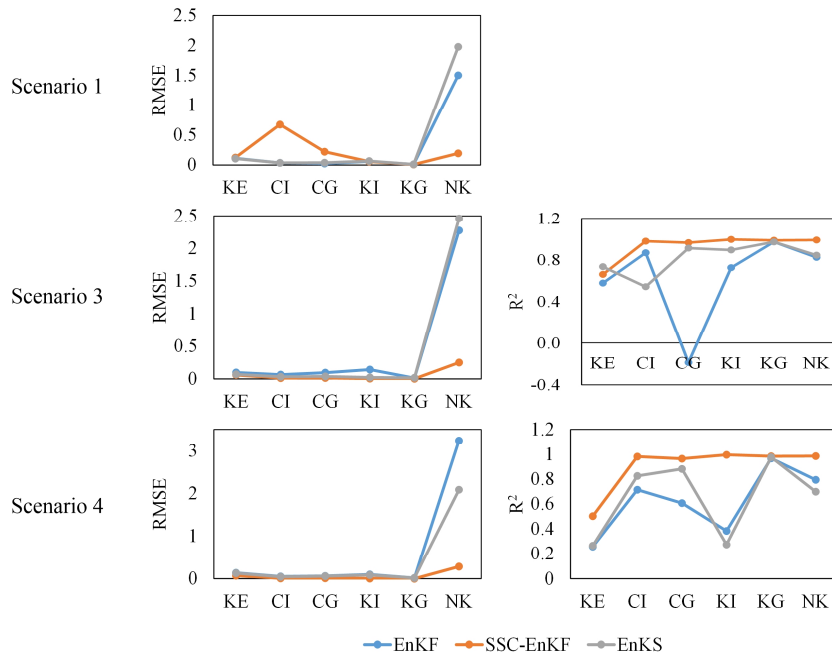


Figure 8 Comparison among EnKF, SSC-EnKF, and EnKS in the synthetic experiment with the Xinanjiang model.



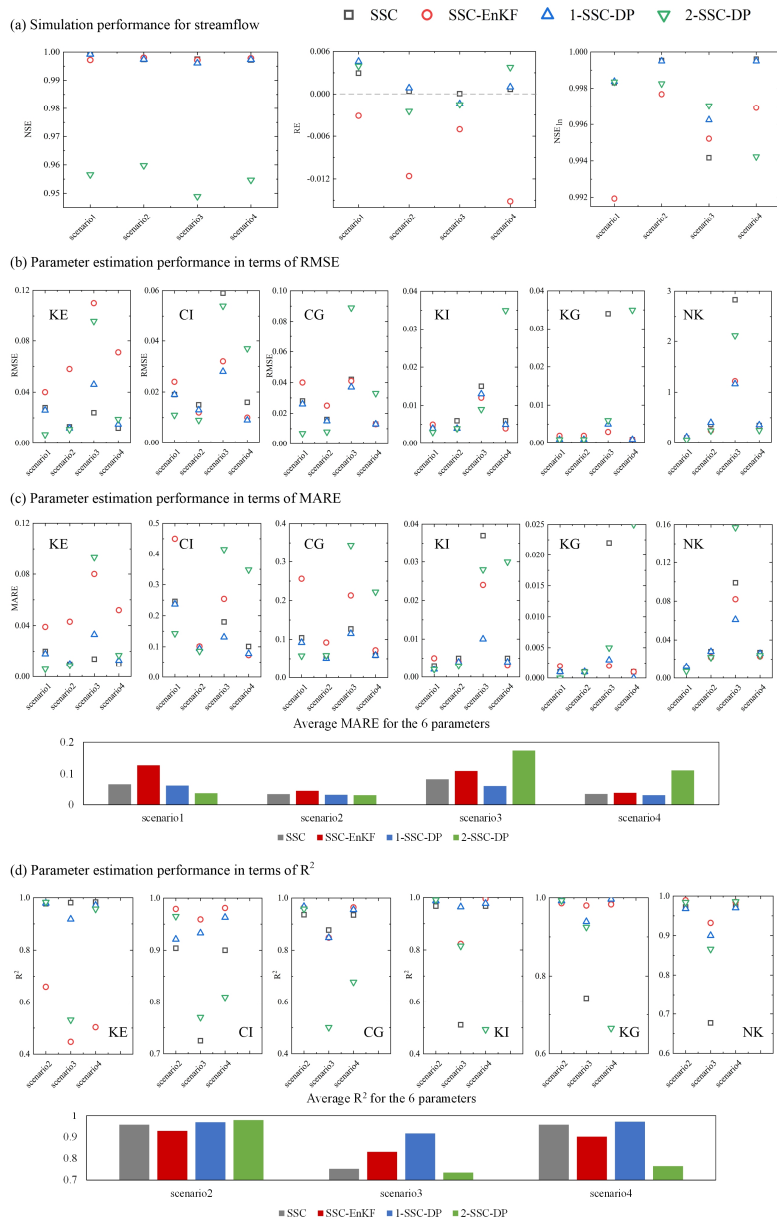


Figure 9 Comparison among the SSC, SSC-EnKF and SSC-DP methods in the synthetic experiment with the Xinanjiang model for (a) streamflow simulation and parameter identification in terms of (b) RMSE, (c) MARE and (d) R<sup>2</sup>.

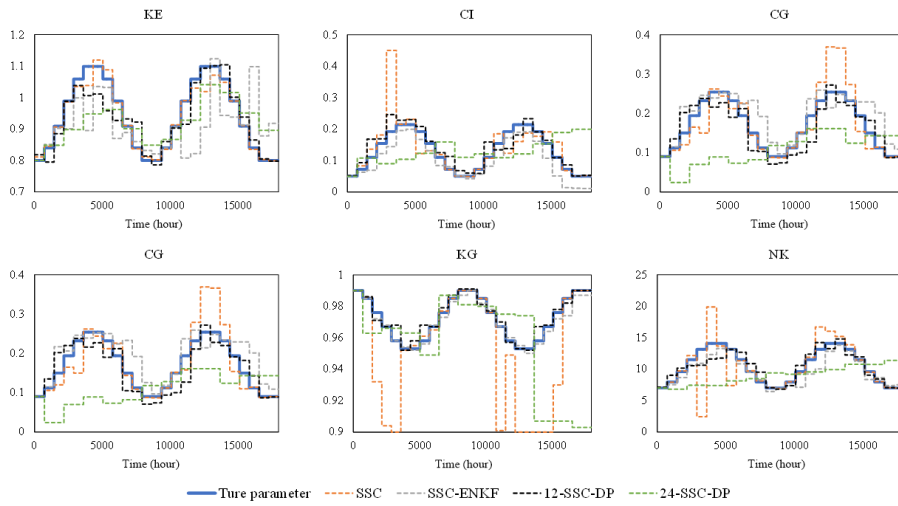


Figure 10 Comparison between estimated parameters and their true values for scenario 3 of the synthetic experiment with the Xinanjiang model.

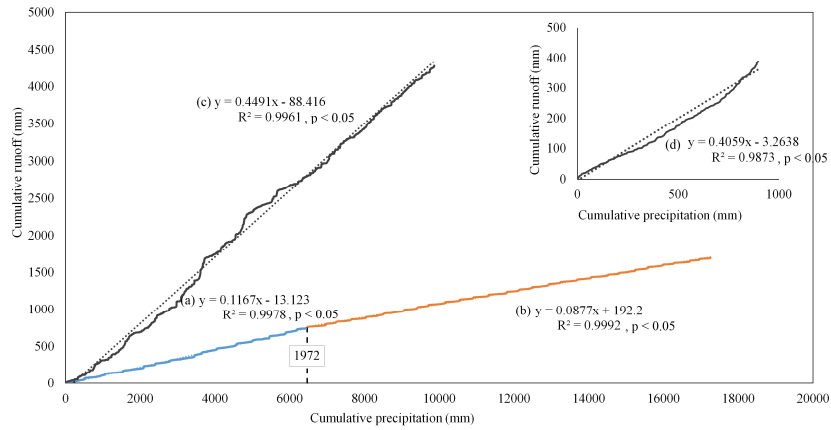


Figure 11 Double mass curves between daily runoff and precipitation for (a) Wuding River basin from 1958–1972; (b) Wuding River basin from 1973–2000; (c) Xun River basin from 1991–2001. Subgraph (d) represents the double mass curve between the mean daily runoff and precipitation from 1991–2001.

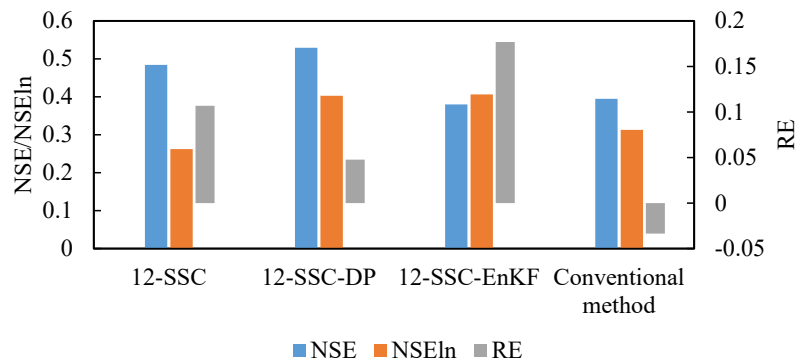


Figure 12 Simulation performance for streamflow in the Wuding River basin. The results of NSE and NSEln are shown on the primary axis, while the values of RE are shown on the secondary axis.

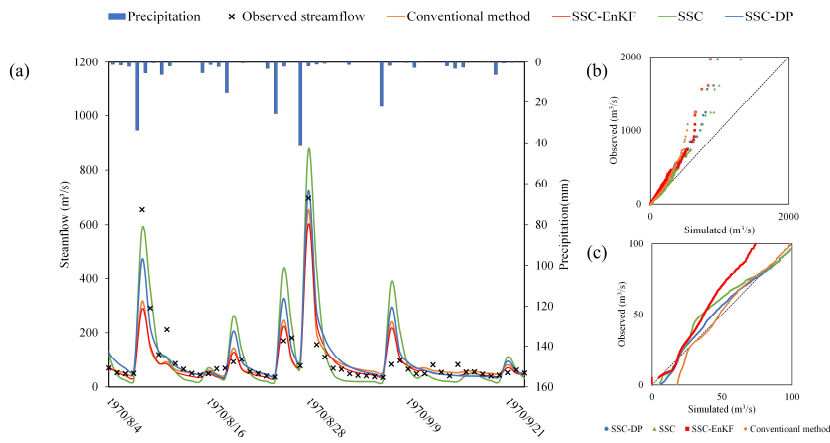


Figure 13 The simulated and observed streamflow using the conventional method, SSC-EnKF, SSC, and SSC-DP for the Wuding River basin. (a) Streamflow simulation hydrograph; (b) The quantile-quantile plot for all streamflow; (c) The quantile-quantile plot for streamflow lower than 100 m<sup>3</sup>/s.

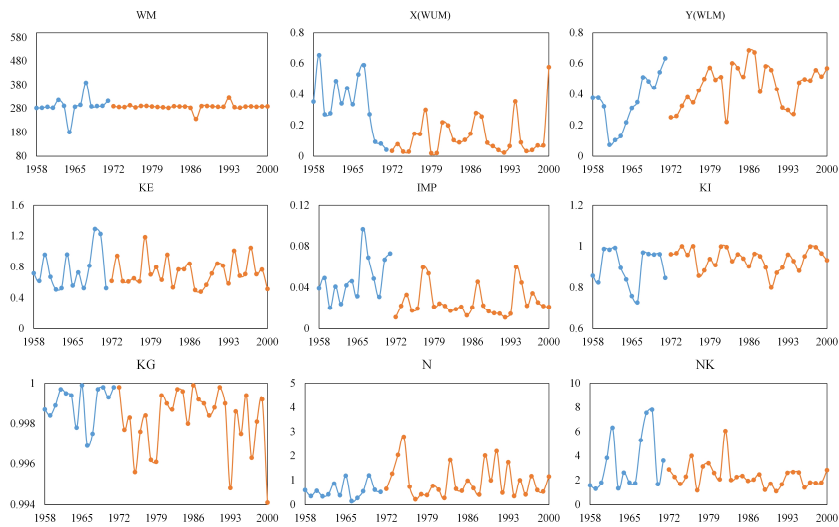


Figure 14 Estimated sensitive parameters of the Xinanjiang model for the Wuding River basin. The blue and orange solid lines represent the estimated parameters pre- and post-1972, respectively.

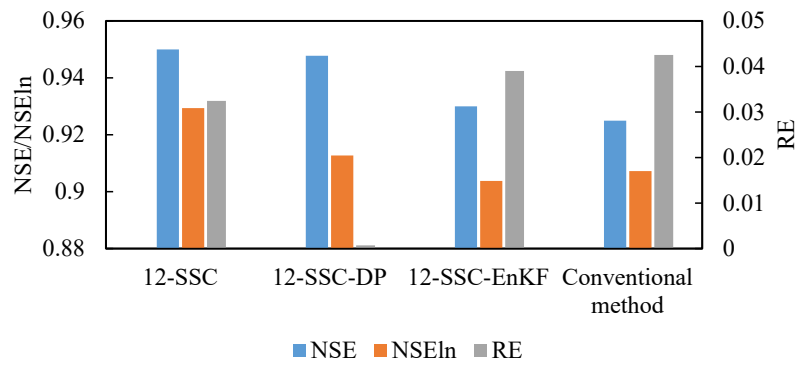


Figure 15 Simulation performance for streamflow in the Xun River basin. The results of NSE and NSEln are shown on the primary axis, while the values of RE are shown on the secondary axis.

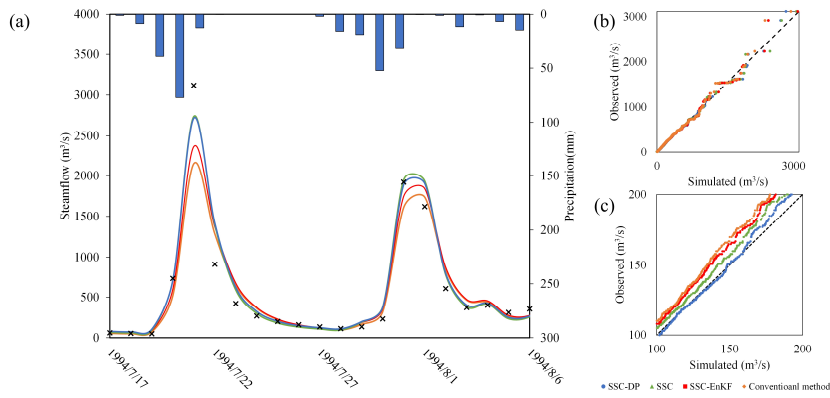


Figure 16 The simulated and observed streamflow using the conventional method, SSC-EnKF, SSC, and SSC-DP for the Xun River basin. (a) Streamflow simulation hydrograph; (b) The quantile-quantile plot for all streamflow; (c) The quantile-quantile plot for streamflow ranging from 100 m<sup>3</sup>/s to 200 m<sup>3</sup>/s.



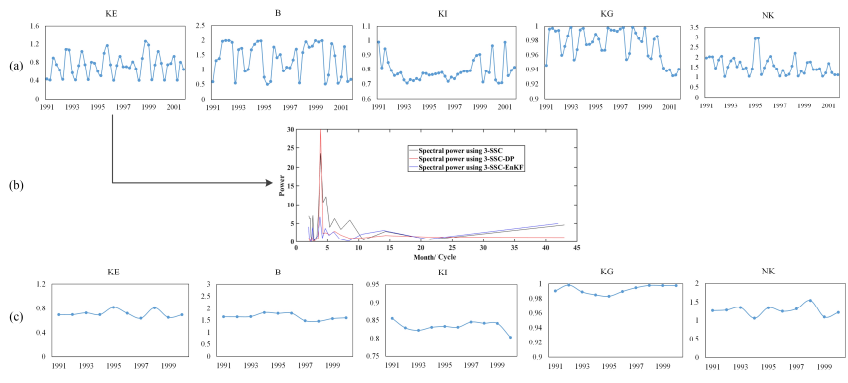
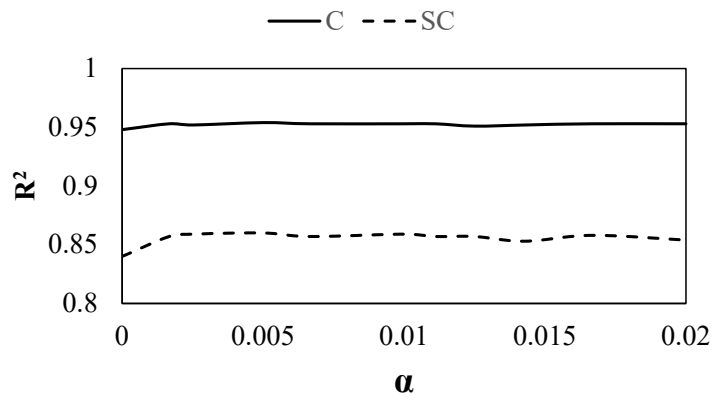
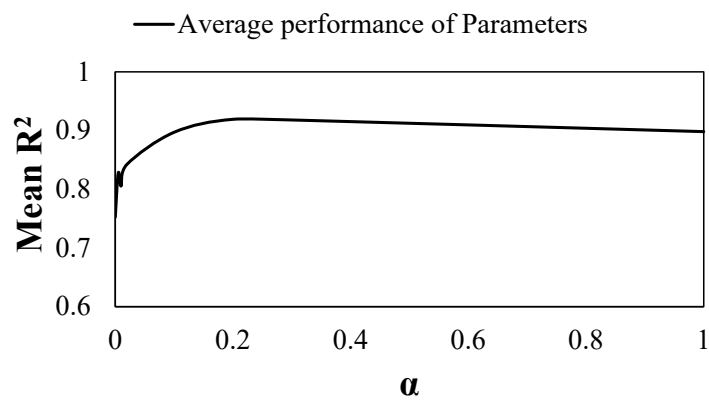


Figure 17 Estimated sensitive parameters of the Xinjiang model for the Xun River basin over (a) seasonal time scale and (c) annual time scale. Plot (b) illustrates the spectral power of parameter KE using different methods.



(a)



(b)

Figure 18 Correlation efficiency results of SSC-DP using different weights of parameter continuity for synthetic experiments with (a) TMWB model and (b) Xinanjiang model. The mean  $R^2$  is the average value of the  $R^2$  such that the identification results for parameters with different ranges can be summarized.